



DTI PhantomMaker: A 3D-Printed DTI Calibration Phantom for Water Diffusion Direction and Anisotropy in the Brain

Permanent link

<http://nrs.harvard.edu/urn-3:HUL.InstRepos:34380097>

Terms of Use

This article was downloaded from Harvard University's DASH repository, and is made available under the terms and conditions applicable to Other Posted Material, as set forth at <http://nrs.harvard.edu/urn-3:HUL.InstRepos:dash.current.terms-of-use#LAA>

Share Your Story

The Harvard community has made this article openly available.
Please share how this access benefits you. [Submit a story](#).

[Accessibility](#)

7	Block Measurement & Analysis	72
7.1.	Anisotropy Measurements and Analysis.....	72
7.2.	Diffusion Direction	77
8	Budget.....	81
9	Conclusion and Future Work	82
10	Acknowledgements.....	84
11	References.....	85
12	Appendix.....	88

Abstract

As diagnostic tools, MRI scanners performing Diffusion Tensor Imaging (DTI) require calibration to ensure standardization. This thesis presents a custom-designed 3D printer used to manufacture a novel type of DTI phantom, which can then provide a standard reference to which machines performing DTI can be tuned.

The phantom is comprised of an array of 3D-printed 1 cm^3 blocks, each of which corresponds to a known value of diffusion anisotropy and direction. In the calibration process, measurements of these cubes from an uncalibrated scanner can then be compared to the blocks' known properties. To achieve blocks of differing anisotropy, the 3D printer mixes fibrous (anisotropic) and non-fibrous (isotropic) polymer filaments in different ratios during printing. To achieve blocks of differing diffusion direction, the block is printed at various oblique orientations in space.

Results from DTI scans of the phantom demonstrate the 3D printer's ability to consistently print blocks of defined diffusion anisotropy and direction, suggesting (1) the viability of this type of 3D-printed phantom in serving as a calibration tool, and (2) the printer's ability to effectively fabricate such phantoms.

1 Introduction

1.1. Problem Statement and Motivation

Diffusion Tensor Imaging (DTI) is a Magnetic Resonance Imaging (MRI) technique used to determine the orientedness, or anisotropy, of nerve tracts within the brain. This technique can be used to diagnose injuries and diseases such as traumatic brain injury, drug use, and tumor formation [1]. In the case of traumatic brain injury, for example, DTI may be used to examine how nerve tracts may have become disorganized and less oriented (i.e. less anisotropic) post-impact [2].

As measurement devices, MRI scanners require calibration to ensure accuracy. Without sufficient calibration, the output of any given MRI machine may differ from that of another, and even the same machine may produce differing outputs over time. This prohibits the accurate comparison of DTI studies across geographies and time periods [3].

Currently, calibration studies necessitate the traveling of human phantoms, who use their own brains as standards across the country [3] [4]. Besides the logistical limitations that prohibit the scaling of this technique as an industry standard, the brain of a human subject is also prone to biological variation over time, complicating standardization [5]. Literature and patent searches show that the American College of Radiology produces a synthetic MRI phantom for machine accreditation; however, this phantom has not been certified for use in DTI calibration [6].

Authors studying DTI accuracy have constructed various liquid chemical-based phantoms [7], though these are complex, hand-made and not intended for commercial use. The lack of a scalable industry standard for DTI imaging is slated to become progressively problematic as DTI becomes pervasive in the field of diagnostic and interventional radiology.

1.2. Target Audience

DTI is a relatively recent technology, having first been characterized in the 1990s with rapid adoption from the 2000s to present [8]. Because DTI can be performed using existing MRI equipment, the market for DTI-related products and services has the upper bound potential to converge with the extremely large MRI market—38.1 units per one million US inhabitants in 2014, or approximately 12,000 units [9]. Though the exact market for DTI is not well-characterized, the number of MRI scanners used for DTI has been rapidly increasing in recent years, and this trend is expected to continue [8] [10].

The primary target end-users for the phantom are the owners/operators of MRI equipment used to conduct DTI studies. Hospitals, imaging centers, and research facilities each require a means to maintain accuracy in their scans. As DTI and similar imaging techniques become ubiquitous, rigorous quality control demands—such as accreditation and ongoing re-calibration—are likely to develop. Thus, the present market need for a scalable, accessible, and cost-effective synthetic DTI phantom follows a positive trajectory.

1.3. Scientific and Technical Background

MRI & DTI Technologies

Magnetic resonance imaging captures the presence of hydrogen protons. This technique is clinically effective due to the presence of hydrogen molecules in water and fat tissues, which are abundant in the body. As an extension of MRI technology, diffusion tensor imaging captures not only the presence of these hydrogen molecules, but also their movement (i.e. diffusion) over short spans of time [1].

Water molecules in brain tissue constantly undergo Brownian-motion based diffusion, which can be described by anisotropy and direction. Anisotropic diffusion occurs along a specific spatial direction, while isotropic diffusion occurs equally and randomly in all directions. Thus, water molecules within structured anisotropic tissues diffuse in a narrow ellipsoid shape, while water molecules within unconstrained isotropic tissues diffuse in a spherical pattern (Fig. 1).

Within white matter tracts of the brain, water moves along the highly organized fibular macrostructure of myelinated axons, resulting in anisotropic diffusion. In contrast, isotropic diffusion occurs within the ventricles, which are larger, unconstrained spaces filled with fluid.

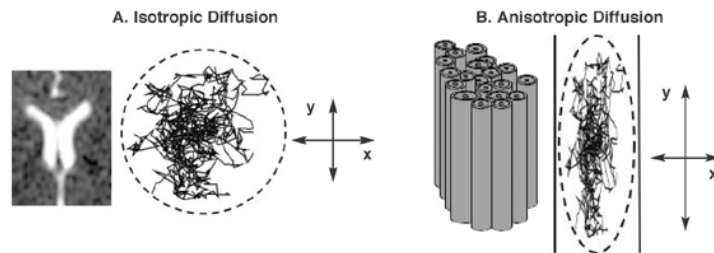


Figure 1. Unconstrained isotropic diffusion in the ventricles (left) results in a circular diffusion pattern, while anisotropic diffusion in white matter tracts (right) results in oriented diffusion. In brain tissue, neuron tracts constrain the diffusion of water, resulting in anisotropy. Image: Rosenbloom et al. [11].

Diffusion tensor imaging captures the anisotropic diffusion of water within axonal tracts and subsequently visualizes the pathways created by myelinated axons [11]. The specific mechanics of diffusion measurement in a DTI study, however, are complex and will not be discussed here.

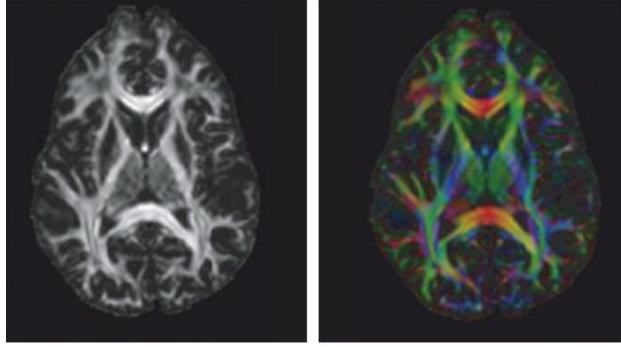


Figure 2. DTI scan of the human brain, depicting tracts of myelinated axons. Bright regions in DTI fractional anisotropy scans (left) and color fractional anisotropy scans (right) represent the diffusion of water in various directions.

Diffusion within a DTI study can be quantified using linear algebra. A diffusion tensor matrix consists of three eigenvectors (v_x , v_y , and v_z) with corresponding eigenvalues (λ_x , λ_y , and λ_z), which represent the direction and magnitude of diffusion, respectively. In anisotropic diffusion, one eigenvalue is appreciably greater than the others, and its corresponding eigenvector corresponds to the major diffusion direction. The ratios of the three eigenvalues are used to calculate a fractional anisotropy (FA) value between 0 and 1, which describes the overall magnitude of anisotropy for a given region [12].

$$FA = \frac{1}{\sqrt{2}} \frac{\sqrt{(\lambda_1 - \lambda_2)^2 + (\lambda_2 - \lambda_3)^2 + (\lambda_1 - \lambda_3)^2}}{\lambda_1 + \lambda_2 + \lambda_3}$$

Based on the above equation, an FA value of zero represents equality among all eigenvalues—meaning diffusion is isotropic, or spherical. An FA value close to one represents dominance of one eigenvalue over the two others, thus describing anisotropic diffusion. In myelinated axons in white matter, one eigenvalue will be much greater than the other two, resulting in high FA values.

Color factional anisotropy (color FA) is a complementary technique that sheds light on diffusion direction, in addition to anisotropy. Color FA is described more fully in Chapter 7.2 of this report.

3D Printing

3D printing is a small-scale additive manufacturing technique that creates objects by laying down successive layers of filament. The filament, or construction material, typically comes in a spool of standard diameter—1.75 mm for this project. The filament is fed into an extruder motor, which uses a sharply-toothed gear to bite into the material, propelling the filament forward due to rotation of the gear. The filament then runs through PTFE tubing from the extruder motor into the hotend chamber, where it is melted. Recently, multiple-extrusion printers have entered the market, which allow for simultaneous extrusion and the mixing of two or more filaments within the chamber.

Molten filament comes out of the hotend nozzle, at which point it attaches to the preceding layer of the object in a process called fused deposition modeling (FDM). Upon cooling, the filament hardens and forms part of the printed object. The hotend is secured onto a moving carriage controlled by stepper motors to enable movement along the x-, y-, and z-axes. In the case of delta-geometry printers, such as the one used in this project, the hotend carriage is suspended on a circular build plate with three pairs of carriage arms attached to vertical guide rails. The triangular configuration of delta printers allows for rapid simultaneous motion in multiple directions. This is in contrast to traditional Cartesian printers, in which axis stepper motors control each axis independently (Fig. 3).

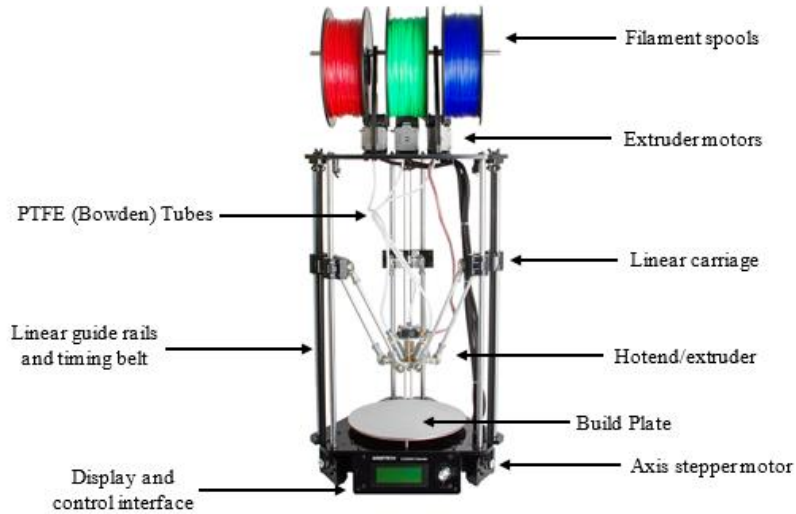


Figure 3. Geetech Delta Rostock 301 printer, a Delta-type printer used in this project.

Within each 3D printing layer, the motion of the hotend during is constrained to the x-y plane parallel to the surface of the build plate. The printer lays down material, layer-by-layer, per a user-specified infill pattern and density. The infill pattern dictates the shape of the internal struts of the object, and common patterns include rectilinear, grid, and honeycomb. The density refers to the spacing in between infill patterns. After one layer is completed, the printer then shifts vertically in the positive z-axis direction to commence the construction of the next parallel layer.

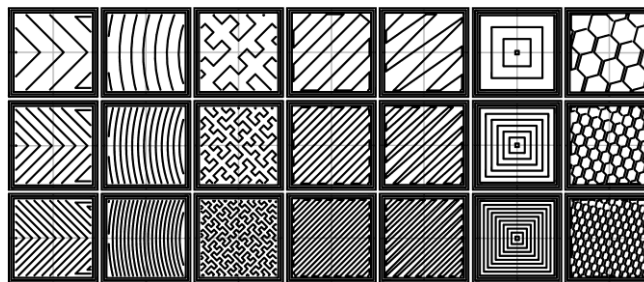


Figure 4. Various infill patterns and densities.

Oftentimes, 3D printers also have the capability to extrude support material that allows for the printing of otherwise unsupported, overhanging layers. Without support material, these elements become unprintable due to the lack of an antecedent layer on which the overhang can be placed. Support material is often made of water-soluble filament such as PVA, which dissolves away when the part is submerged in water. Support filament is often extruded through the same nozzle as the printing material.

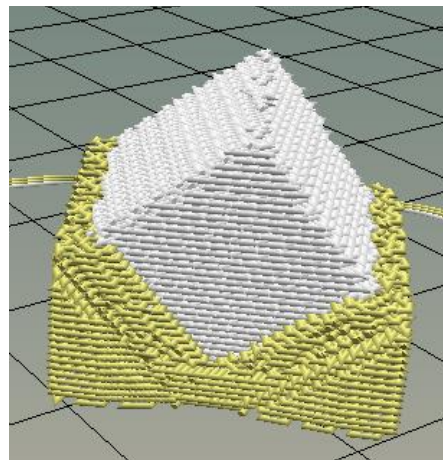


Figure 5. CAD rendering of white block printed on an edge. Yellow PLA support material, which dissolves when placed into water, allows the printing of the white block's overhanging structures.

All printer movement is computer-controlled by means of G-code. To begin the printing process, a 3-D computer design file (usually an STL file) describing the overall shape of the object is loaded into slicing software. The software then analyzes the part and generates corresponding machine code according to user-defined slicing/print settings. Settings such as infill percentage, infill pattern, hotend temperature, bed plate temperature, the architecture of support material influence how the part is printed.

2 Design Goals

This thesis expands on the ongoing work of the Simulation Group (SimGroup) at Massachusetts General Hospital. The aims of this project are twofold: (1) Construct a 3D printer capable of printing DTI calibration phantom components, and (2) fabricate the DTI calibration phantom itself and test its viability for use as a calibration tool. These two aims are described in the following sections.

2.1. Phantom Design Goals and Specifications

Phantom Structure Design

The end-goal design originally proposed by the SimGroup at MGH consisted of an assembly of 150-200 1 cm^3 cubes that form a synthetic brain “slice.” The synthetic slice would model the diffusive properties of actual human brain tissue, as each cube would be printed such that the water diffusivity of any given block matches the diffusivity of brain tissue in the corresponding region. Thus, one would expect a cube in the center of the phantom to exhibit isotropic diffusion as it recapitulates the free diffusion of cerebrospinal fluid within the brain’s central ventricles.

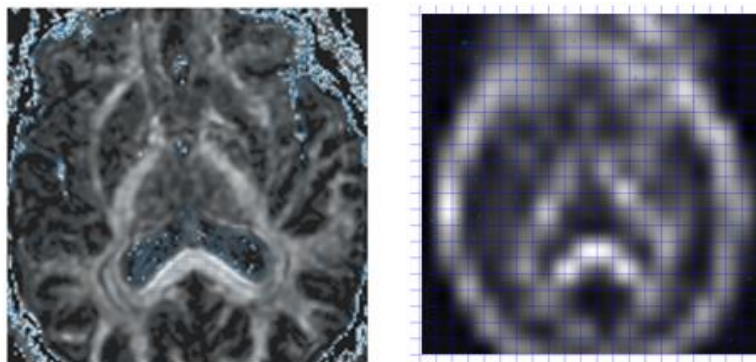


Figure 6. Raw DTI image with high resolution (left). Voxels are then averaged to generate one representative value for anisotropy and direction for each 1 cm^3 cube, decreasing the resolution (right). Overlaid grid not to scale.

The design of the phantom, however, was modified throughout the experiment. The original design was simplified to a small cube of 27 blocks (Fig. 7), as phantoms need only contain specific representative values that fully characterize the range of measurement. The revised design captures three different anisotropy values and linear combinations of all directions.

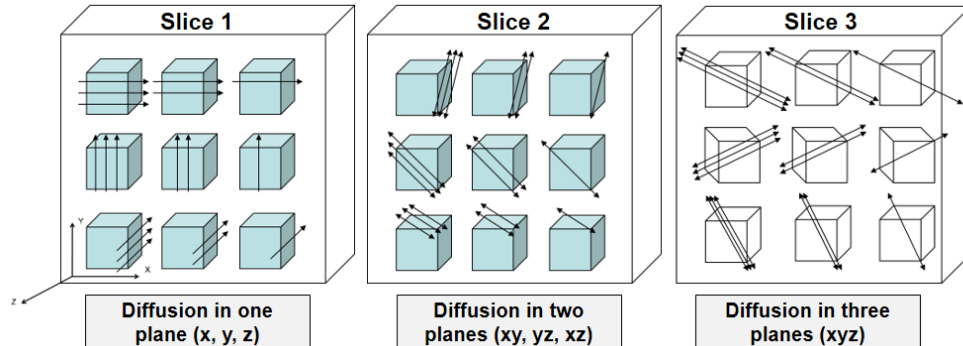


Figure 7. Revised phantom design consisting of a 3x3x3-block cube, broken into slices in the above image. The number of arrows correspond to the amount of anisotropy, while arrow direction represents the direction of diffusion. Each successive slice incorporates linear combinations of various directions, fully characterizing diffusion in 3D space.

The blocks must therefore effectively capture the biological range of diffusion anisotropy values, typically in the 0.4 to 0.7 range [11]. Additionally, in the case of anisotropic diffusion, the cubes must capture the spatial direction of the diffusion. In quantitative terms, each cube will represent any given fractional anisotropy (FA) value within biological range and any arbitrary 3-dimensional spatial orientation vector.

The cubes, after being infiltrated with water, are to be resistant to deformation, degradation, and dissolution when exposed to excessive moisture for long periods of time. As a calibration device, it is essential that the diffusive properties of the phantom remain constant over time. The phantom need also be nonferrous, as MR imaging employs strong magnetic fields.

Phantom Material Design

To produce cubes of varying anisotropies, two filaments of different anisotropies are mixed in varying ratios. One such material is Lay-felt [13], a synthetic fiber material made of a rubber-elastomeric polymer and PVA. Preliminary investigations by the SimGroup have demonstrated that objects printed with Lay-felt result in anisotropic diffusion along the printed fiber direction. In contrast, Gel-lay [14], made of another type of rubber-elastomeric polymer with PVA, is believed to result in more isotropic diffusion. By varying the mixing ratio of Lay-felt and Gel-lay during 3D printing, blocks of differing anisotropies can theoretically be fabricated.

The anisotropic and isotropic character of Gel-lay- and Lay-felt-printed objects become activated after placing the object in a water bath for 1-4 days. During this time, the water-soluble PVA carrier filament dissolves away, leaving behind the relevant Gel-lay and Lay-felt polymer material.

Diffusion Direction

In this project, each block only represents one diffusion direction, and so all fibers within the block must be oriented in the same way. The infill pattern of the block thus consists of parallel lines, and water diffuses within the tracts created by these lines.

When Lay-felt/Gel-lay blocks are printed with the bottom block face completely in contact with the build plate, the block's tracts are either parallel or perpendicular to any given block edge.

This non-rotated block allows for diffusion in a singular axial direction, from one block face to the opposite.

However, because diffusion rarely happens in a singular x-, y-, or z-direction, the fabrication of blocks of arbitrary orientation is necessary. This is achieved by printing the blocks in an oblique

orientation. In this process, no face of the block comes in full contact with the build plate itself. Instead, printing begins at an edge or corner and continues upward, layer-by-layer, in the z-direction. After printing, the block is then rotated back to a normal position in which one face is fully in contact with the build plate. When viewed from this perspective, the fiber tracts are diagonally-oriented relative to the build plate. Blocks printed in this manner require support structure on the bottom portion of the part, since the outside edges of bottom layers are unsupported by the preceding layer.

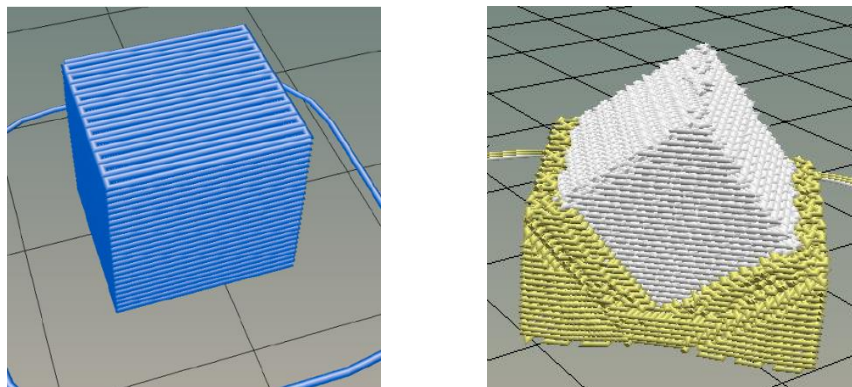


Figure 8. A non-rotated block (left) is printed with one face in contact with the build plate, resulting in fibers parallel or perpendicular to block edges. Diffusion occurs only in the x-direction along the tracts. A rotated block (right) is printed starting at an edge or corner, resulting in diagonal tracts when rotated back to a normal position. Diffusion occurs in the x-, y-, and z-directions along the tracts. In both cases, each successive layer of parallel infill lines remains parallel to the antecedent layer during printing.

Suspension Medium Design

It is important to note that Lay-felt and Gel-lay, as fibrous polymers, do not inherently contain water. Instead, these blocks simply provide a structure in which water can diffuse. Water must be introduced around the blocks so that hydrogen molecules can infiltrate into each block, generating diffusion measured by DTI. Therefore, after the blocks are printed, they must be supported in a hydrated suspension medium. The purpose of this medium is twofold: 1) to

provide a saturated source of water molecules that diffuse in and out of the blocks, and 2) to fix the individual blocks in space.

Scanned objects that contain too little water generate an insufficient signal to be identified by the MR scanner, and the scan will not execute. Furthermore, to allow for the observation of unobstructed diffusion in all directions, the cubes must be also *suspended* in a hydrated medium, away from obstructions such as container walls and other blocks. The suspension medium must therefore be sufficiently hydrated, yet resist the motion of blocks due to gravity and movement of the phantom.

2.2. Printer Design Goals and Specifications

To accommodate the simultaneous extrusion of two different filaments as well as support structure, the printer must be able to extrude three separate filaments. Additionally, the printer must be able to mix the two molten filaments together to create a homogenous mixture, which can then be extruded to construct the print.

The printer needs to seamlessly switch between print material and support material, ensuring that cross-contamination does not occur. The introduction of support material residue in the block itself will cause defects as the support material dissolves away when exposed to water.

Because cubes will only measure 1cm per side, the printer must be able to consistently and accurately execute small-scale movements. High precision is needed as DTI is sensitive to variations, and inadequate print quality or consistency directly hinders the usefulness of the device as a DTI phantom.

3 Design Approach

This section introduces the decision-making processes that informed the original, general design of the printer and phantom. Section 3.1 describes why the option to modify a stock printer was chosen over others. Section 3.2 discusses the general approach to the construction of the phantom, while Section 3.3 discusses software.

3.1. Printer Selection

The market lacks a ready-made 3D printer that meets the specifications described in Chapter 2. Thus at least some element of modification and original design will be required to construct an appropriate device.

In the printer selection process, three options were considered:

- Construct a new, custom printer entirely from scratch with raw materials
- Construct a new printer based on open-source 3D printer designs and modify as necessary
- Modify an existing Makerfarm Prusa i3 printer, already in the lab's possession
- Purchase a new printer and modify as necessary

In selecting the appropriate option, the following criteria were considered:

- Amount of modification needed to achieve custom specifications—and as a corollary, time to completion
- Level of specialized technical expertise required
- Reputation, quality, reliability, and durability of printer
- Cost

Each of the above options were evaluated per each of the criteria and summarized below.

Building Printer from Scratch

Benefits: High degree of customization, lower cost

Drawbacks: Very high specialized technical expertise required, potential for quality issues, time-consuming

Comments: The very high specialized technical expertise required was prohibitive. Custom-building 3D printers from scratch is typically an activity attempted by 3D printing experts. Given the lack of long-term experience, an attempt to build a printer from scratch runs the risk of a poorly constructed printer. The time required to learn, design, and build the printer is also prohibitive. Furthermore, no official or community support exists for non-standard printers.

Building Printer from Open-Source Designs

Benefits: Medium-high degree of customization, lower cost

Drawbacks: Specialized technical expertise required, potential for compatibility issues, time consuming—though less so than building printer from scratch

Comments: Though many printer designs are available for use online, high levels of technical expertise are still required to construct a new 3D printer. Online designs may also not meet specifications, which requires that designs undergo time-consuming modifications. Though preferable over a printer entirely from scratch, the level of time and expertise required with high risk for failure is prohibitive.

Fix & Modify Existing Makerfarm Prusa i3

Benefits: Basic printer already in place, low cost, less time and technical expertise than build-your-own

Drawbacks: High level of modification needed, compatibility issues, risk for existing problems to remain

Comments: This printer had been used previously in attempting printing Gel-lay and Lay-felt. Lay-felt had failed to print, and dual-extrusion did not function. Further modifications would require the installation of a triple-extrusion hotend that can accommodate three different filaments, the installation of another extruder motor to accommodate the third filament, and the installation of a new controller board and firmware to accommodate the extra hardware. Further, compatibility of the new components with the Prusa i3 was not known.

Purchase and Modify New Printer

Benefits: Can purchase new printer with specifications already close to our needs, requiring fewer modifications; technical support available; requires relatively less time and expertise

Drawbacks: Cost, quality (given budget constraints, printer will not be high-end)

Comments: Preliminary product searches, conducted with a \$500 cost cap, identified one particular printer as being a strong candidate. Purchasing the Geeetech Delta Rostock 301 printer for ~\$430 would be a more expensive option, though would still keep the project under budget. The printer would be pre-packaged with triple-extrusion and mixing capabilities. Quality is a concern due to the low cost and reputation of the manufacturer. Significant expertise is not required for assembly, though major modifications may be needed.

The construction of a new printer, either from scratch or with open-source designs, would require prohibitive investments of time and effort. Furthermore, the expertise required is beyond the scope of this project. Thus, any option involving the custom-building of a 3D printer was eliminated early in the design process.

Ultimately, the decision was between modifying the existing Prusa i3 printer and purchasing and modifying a stock printer. Through a full online product search and discussions with 3D printing experts within the lab, the only low-cost printer capable of simultaneous-mixing and triple-extrusion found on the market was the Geeetech Delta Rostock 301.

The most critical criterion is support for triple extrusion and simultaneous mixing. In regards to this criterion, the Geeetech printer was ultimately selected due to its “all-in-one” nature, being marketed for intended use as a triple-extrusion printer. The Prusa i3, in contrast, would need to be retrofitted for a triple-extrusion hotend and more extruder stepper motors, which runs the risk of compatibility issues.

Both printers would have required the installation of a new build plate fan and modification of firmware to accommodate G-code based mixing. However, the closed-source nature of the Geeetech printer’s firmware and controller board was not evident at the time. Information

regarding the printer’s mechanical stability in regards to small parts fabrication was also not known, as literature and end-user reviews on the printer were sparse. At decision time, it was expected that the Geeetech printer would require the least amount of modification to achieve the required specifications, with the lowest amount of risk due to the inherent mixed-extrusion design of the printer.

From a cost perspective, the entire printer seemed like an excellent value at the time of purchase. Modifying the existing Prusa i3 printer would have required ~\$200 in new parts, as a new hotend, extruder motor, and customization hardware would have been required. It was determined that the higher cost of buying a new printer was justifiable given the ostensible savings in time, effort, expertise, and risk.

These considerations are outlined in the options table below.

	Printer from Scratch	Open-source design	Modify Prusa i3	Modify new printer
Modifications/time req’d	Very high	Very high	Moderate	Lower
Expertise required	Very high	Very high	Moderate	Lower
Quality risk	High-risk	High-risk	Moderate risk	Moderate risk
Cost	Lower	Lower	Moderate	Higher

Table 1. Design options analysis of various printer construction approaches.

In light of this decision-making process, the Geeetech Delta Rostock 301 printer was purchased from the manufacturer in October 2016 and arrived via overseas shipment in November.

However, significant printer quality issues and software limitations were discovered during the building and testing processes, which required extensive printer modifications and re-designs.

These modifications are described in Chapter 4.

3.2. Phantom Material Selection

An investigation of the properties of Lay-felt and Gel-lay were conducted prior to my arrival on the project team. As the Lay-felt and Gel-lay materials were selected prior, the material selection process centered on the cube support material and phantom suspension medium.

Cube Support Material

The cube support material must be water-soluble to facilitate removal post-print. Furthermore, the printing temperature must be close to that of Gel-lay and Lay-felt, approximately in the range of 225°C. A common reliable material is polyvinyl alcohol (PVA), which readily dissolves in water and has a recommended printing temperature of 190°C - 220°C.

Because the support filament and print filaments are often both extruded within the same layer, only one print temperature can be configured. Extrusion of this material was tested at 225°C, the recommended print temperature of Gel-lay and Lay-felt, despite being slightly above the suggested range. However, printing was successfully with no noticeable compromise of print quality. Because of the accessibility, reliability, and compatibility of PLA, it was selected as the support material.

Phantom Suspension Medium

To create a sufficiently large hydrated medium to suspend the blocks, several design ideas were considered. An earlier study conducted by the Group involved placing blocks in a plastic soda bottle for scanning. However, because the test blocks floated within the bottle, diffusion was restricted in the positive-z direction. Furthermore, the soda bottle did not contain enough water to generate a machine-detectable signal. This demonstrated that further designs would require 1)

the suspension of the blocks in the center of the water-based medium to permit free diffusion of water in all directions, and 2) the incorporation of more water volume.

In the suspension medium selection process, the following criteria were considered:

- Abundance of water molecules
- Allowance of the free diffusion of water in and out of block from all directions
- Ability to maintain block structural integrity
- Ease of production and implementation (e.g. arranging and replacing blocks)
- Durability and structural/chemical integrity over time

In the brainstorming process, the following ideas were considered as candidates:

- Stringing a fishing wire through the centers of the cubes, which will then be stretched from one end of a water-filled vessel to another
- Using sheets of low-density radiotransparent webbing above and below cubes to maintain cube position
- Creating a water-based hydrogel of high viscosity to secure cubes in suspension

Of the three options above, stringing the blocks together using fishing wire was quickly eliminated as the least workable solution. To do this, a small gap would have to be made in the center of the cube. This would require the tedious, manual modification of block G-code, and the discontinuity within the block may impact structural integrity. This gap would also affect the homogeneity of the block, potentially affecting diffusion measurements. Lastly, while the blocks may be tethered against the effects of gravity and buoyancy, they are still free to move about the fishing line, which creates directional inconsistencies. This option represented a relatively high-risk, high-effort, and low-reward scenario.

The webbing design consisted of two layers of radiotransparent mesh. The mesh would act as barriers to the z-directional movement of the blocks sandwiched between them. This design

failed in its ability to keep the array of the blocks from shifting between scans, as the blocks would remain unsecured in the x-y plane. Furthermore, the integration of the webbing within a liquid vessel would require more complex design considerations: a bottom layer would need to be secured to the vessel walls while the top layer would need to be easily removable for cube placement.

Creating a water-based hydrogel to suspend the blocks emerged as a superior design. Hydrogels are relatively inexpensive and commercially available. The high viscosity of hydrogel accommodates block suspension with minimal movement within the medium. Hydrogels, which consist of mostly water, should also allow for the diffusion of water molecules into and out of the blocks. Because of its simplicity and cost-effectiveness, this design was ultimately selected.

The below table summarizes the design considerations for the phantom suspension material. For each option, any unfavorable rating would disqualify the design, as each criterion was necessary for the fabrication and proper function of the phantom.

	Maintains block integrity	Ease of fabrication and implementation	Permissibility of omnidirectional diffusion	Maintains block position
Free-floating within plastic bottle	Favorable	Favorable	Unfavorable	Unfavorable
Blocks secured with fishing wire	Unfavorable	Unfavorable	Favorable	Unfavorable
Blocks secured with top/bottom mesh	Favorable	Unfavorable	Favorable	Neutral
Blocks suspended in viscous hydrogel	Favorable	Favorable	Favorable	Favorable/neutral

Table 2. Design considerations of phantom suspension material against critical criteria.

Hydrogel Suspension Design

The specific chemistry of hydrogel was determined based on the availability of materials in the lab. Carbomer 940—formally known as poly(acrylic acid) (PAA)—was readily available in the lab, and studies have shown its viability as an MRI phantom material [15]. The electrolytic chemistry of Carbomer renders it hydrophilic, with the ability to swell and absorb water.

The hydrogel was made using a standard preparation of 0.4% Carbomer powder by weight. To create one liter of hydrogel, 4g of dry Carbomer powder was added through a sieve (to prevent clumping) to 1L of tepid water. During Carbomer powder addition, the water was placed on a stir plate to promote rapid dissolution. After the addition of the powder, stirring continued at a medium speed for an additional ~5 min. The solution was then neutralized with ~2 mL triethanolamine, a base, and left overnight to thicken. As triethanolamine was added, the pH of the solution was tested, ensuring that a neutral pH (~7-8) was ultimately achieved.

Hydrogel Suspension Prototype & Testing

To validate the ability of the hydrogel to properly suspend cubes and provide a source of water molecules, a small sample was first tested in a 50mL syringe with 4 printed cubes. The first trial scan revealed that this small amount of gel would not produce an adequate signal for scanning. To compensate, the syringe was taped to a large container of MRI fluid, after which the scan successfully executed.

Results from this scan reveal appreciable diffusion within the blocks (Fig. 9), demonstrating that the hydrogel could sufficiently provide a source of water. The ability for the hydrogel to securely suspend the blocks was tested by placing one block in a syringe and measuring its movement over time due to gravity or buoyancy. The block did not move over the course of five weeks,

demonstrating the spatial stability of blocks within the gel. Furthermore, no bacteria growth was noted within the hydrogel within five weeks, a promising and important property, as hydrogels are often prone to the growth of bacteria [16]. This prototype strongly validated the hydrogel as a suspension medium for the phantom. Design details of the hydrogel suspension used in the prototype phantom are found in Chapter 6 of this report.

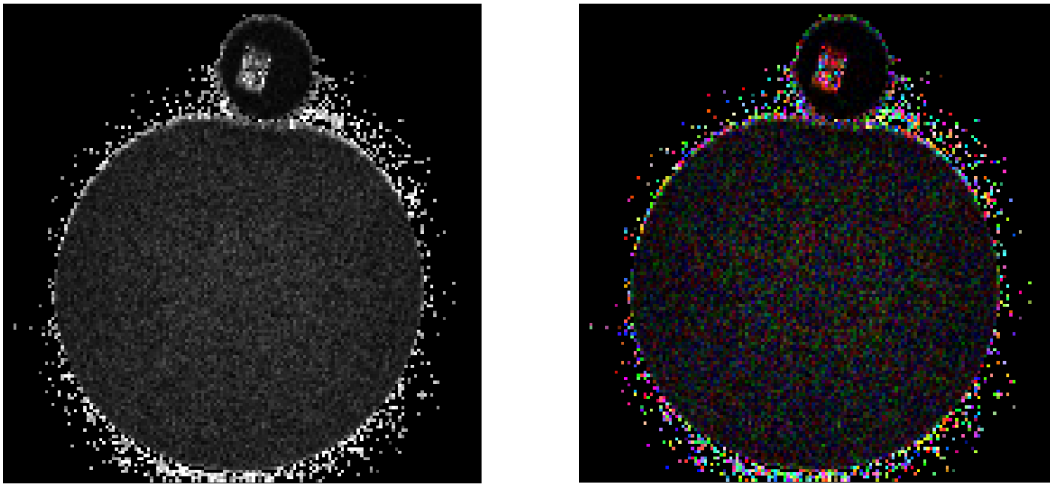


Figure 9. Cross-sectional view of hydrogel prototype. Bottom circle in image is large container of MRI fluid, necessary to generate sufficient diffusion signal. Top circle is syringe cross-section with one block. FA (left) and color FA (right) demonstrates appreciable diffusion of water, demonstrating proof-of-concept.

3.3. Software Selection

This project involves four different software elements. The process begins at the generation of an STL file using computer-aided design software. The STL file contains information about the geometry of the object. This then gets loaded into slicing software, which generates machine-readable G-code based on the STL file and user-defined print settings. Many settings, such as printing temperature, filament density, and print speed, are individually adjusted based on the material, application, and desired object properties. Next, host (or control) software sends this G-

code to the printer while also providing a graphical user interface to translate manual human commands into machine-interpretable commands. Lastly, the G-code is received by the printer firmware located on the printer's controller board, which translates machine commands into physical motions of printer components. This process is outlined in the diagram below.

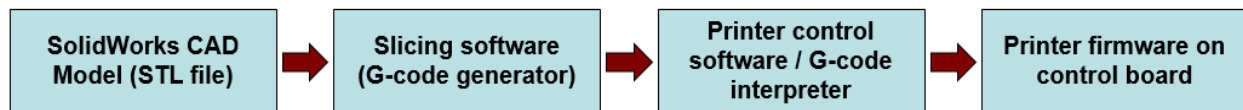


Figure 10. Overall workflow of 3D printing software. Each individual software component requires selection and configuration.

In this section, the selection process of each software component will be discussed. Specific software settings and configurations will be discussed in Chapter 5.

Computer-Aided Design Software

For this project, SolidWorks was used as the 3D model generator. SolidWorks has become a de facto standard for computer-aided design in the engineering and 3D printing industries [17].

While SolidWorks is considered professional software, this project does not require complex 3D modeling. Though other popular software packages, such as SketchUp Make, are more accessible in terms of cost and beginner use, the availability of the SolidWorks academic license and the team's extensive familiarity with the software rendered it a natural choice.

Slicing and Printer Host Software

The slicing and printer host software selection process focused on cost-benefit and availability of documentation. Three major slicing software packages were tested: Slic3r, Cura, and Simplify3D. The former two were selected because of the printer manufacturer's recommendation and previous work done with the software within the Group. These two pieces

of software are free and have fully been integrated within Repetier-Host, the manufacturer-recommended printer host software. Simplify3D was later considered after a literature search revealed its superior capabilities to slice prints based on the project's needs. However, it was a last-resort consideration due to its \$150 license.

Repetier-Host was first used as the printer host software. Within Repetier, the integrated Slic3r was used as slicing software. These two programs were selected due to (1) the printer manufacturer's recommendation, and (2) the Group's previous experience with the software packages. Using Slic3r, the G-code for the non-rotated cubes was generated per the settings found in Appendix 12.1. This G-code, found in Appendix 12.2, would become the standard for all non-rotated cubes.

However, as the project progressed into the printing of rotated cubes, it became evident that Repetier-Host and Slic3r did not provide all needed functionality. Specifically, Slic3r did not allow for the incorporation of a priming pillar, which is necessary to print support material and the block itself simultaneously. Without a priming pillar, support material would blend with cube printing material in the hotend and extrude simultaneously—resulting in cubes that are contaminated with PVA and, vice versa, support material that was contaminated with Gel-lay or Lay-felt. The incorporation of a priming pillar provides an area where the unwanted, mixed filament intermediates can be discarded in between filament changes.

After a literature review, it became evident that two other pieces of popular commercial slicing software offer the capability to incorporate a priming pillar: Cura and Simplify3D. However, after extensive testing, it was discovered that Cura does not support an object perimeter value of

zero, which is a necessary specification for the cubes.¹ Instead, Simplify3D software was ultimately used. Simplify3D integrates both host software and slicing software, and a copy of the paid license was borrowed from Dr. Damien Galanaud in the Group. Future developments of this project may require the purchase of this software for \$150.

Printer Firmware

The original controller board packaged with the Geeetech printer contained a closed-source, proprietary firmware. However, during the build phase, it became evident that this firmware does not support G-code commands for mixed extrusion. Therefore, the firmware needed to be replaced. This also necessitated the complete replacement of the controller board, as it is also closed-source.

Currently, two major open-source firmware packages support mixed extrusion: Marlin and Repetier. The replacement RUMBA board is compatible with both, and extensive documentation exists for both [18]. Marlin was chosen due to the relative expertise of the SimGroup team in configuring the firmware, and of the available versions, Marlin 1.1.0-RCBugFix (December 2016) was selected due to recent upgrades to its multiple-extrusion capabilities [19].

¹ An external perimeter is a circumferential, continuous layer of filament designed to provide external structure to the print and contain the patterned, porous infill material. However, in this project, an external perimeter would “seal” the block and prevent the free diffusion of water into and out of the cube. Therefore, a perimeter is not desired.

4 Printer Build & Design Evolution

Based on the Design Approach discussed in Chapter 3, a stock Geeetech Delta Rostock 301 printer was purchased with project funds. Though originally minor modifications—such as the integration of a print bed fan—were anticipated, the extent of modifications eventually performed far exceeded initial estimates. This made the printer build process extremely iterative, as many eventual design elements revisions were not originally considered due to 1) the lack of robust documentation on the printer, and 2) unanticipated quality issues.

The general process for the testing and building of the printer is described in the block diagram below. Block elements from left to right represent increasing complexity, with each numbered block element representing a Build Phase. The printer was originally designed to extrude conventional materials such as PVA and ABS, and initial testing began at Build Phase 1. The printer build culminated in the ability to successfully print the most complex type of block needed for the phantom: a mixed-extrusion block in an arbitrary orientation, which requires the seamless integration of support material during printing.

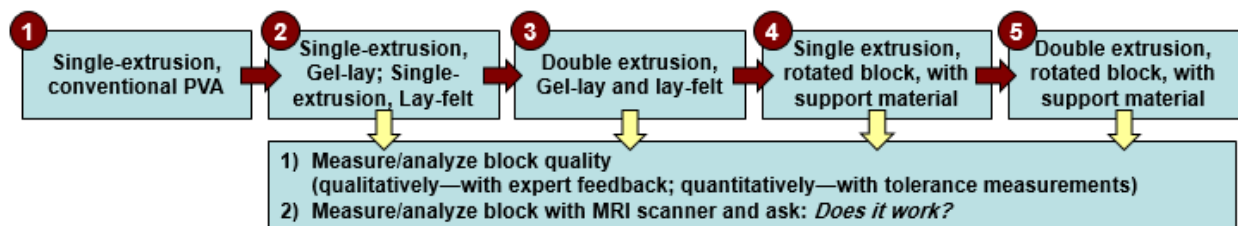


Figure 11. Printer build process diagram, from Build Phase 1 (least complex) to Build Phase 5 (most complex).

At each Build Phase, the printer was tested by printing the corresponding type of block. During printing, printer issues that prevented the successful printing of the block were identified and subsequently addressed per the framework described in Figure 11. After successful printing was

achieved, block quality was assessed qualitatively through inspection and quantitatively through tolerance measurements. Many block issues, however, could be identified directly based on careful observation without the need for further time-consuming quantification. Common issues included curved edges, poor layer adhesion, underextrusion, and warping.



Figure 12. Within each Build Phase, an iterative Design-Build-Measure/Analyze process allowed for the implementation of the status quo design followed by an evaluation of the printed blocks and subsequent design revisions.

After multiple iterations of the above process, many major changes to the design of the printer were made. A chronological summary of the design evolution is summarized the diagram below.

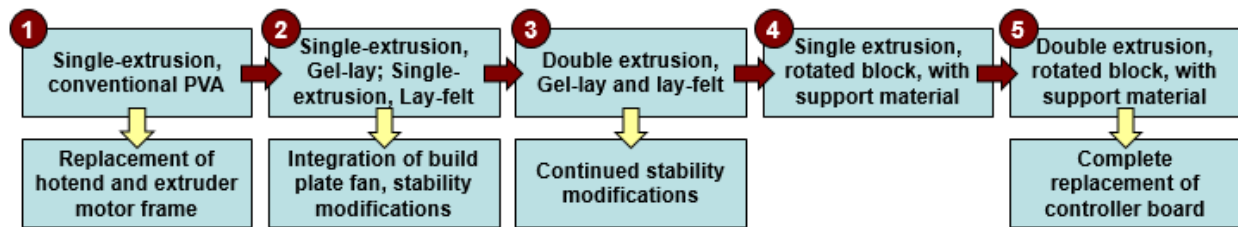


Figure 13. Each Build Phase illuminated shortcomings in the original printer design that required subsequent design modifications, which are described by the bottom row of boxes.

The details of each modification will be discussed in the following sections.

4.1. Initial Construction and Testing

Initial Stock Assembly and Set-up

Initial construction of the Geeetech Delta Rostock 301 printer was completed according to the manufacturer's instructions without significant issue. Upon assembly, the printer successfully turned on and moved to a home position.

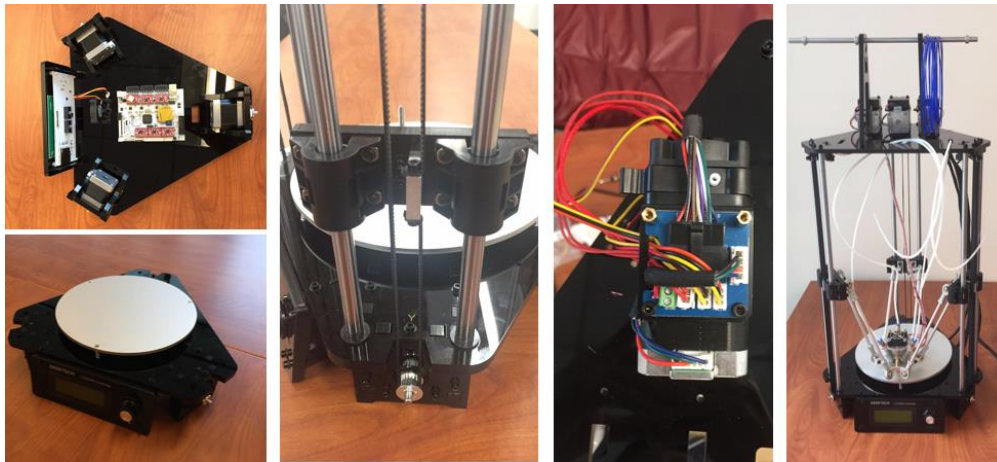


Figure 14. Selected images of the build process. The printer arrived completely disassembled in its constituent parts. From left to right: Base plate assembly (top and bottom images), axis carriage assembly with timing belt and linear guide shaft, original extruder motor and electronics, completely assembled printer (excluding power supply).

Bed leveling was performed according to the manufacturer's specifications; however, this proved to be an extremely time-consuming process. This process involved placing a sheet of printer paper on the print bed and bringing the heated print nozzle down to a z-axis height of 0 mm, effectively sandwiching the sheet of paper between the nozzle and the bed. Three leveling screws on the bed plate and three endstop screws were then minutely adjusted based on the amount of tension on the paper when pulled. Ideally, the tension caused by the nozzle against the paper should barely allow for the back-and-forth movement of the paper when moved by one hand. An inability to move the paper with one hand meant the tension was too high. In response, the

nozzle must be lifted relative to the bed plate by either loosening the bed plate screws (which elevate the bed plate) or the tightening the endstop screws (which effectively lower the nozzle after homing). In contrast, the complete free movement of the paper beneath the nozzle indicates that the nozzle was too high and not in contact with the bed plate at the $Z = 0$ position. In response, the nozzle should be lowered relative to the bed plate. This process began at the center of the bed plate and proceeded around the circular bed plate around its edge by manually moving the hotend with the printer control software.

Because every endstop screw adjustment affects the relative “home” position of the nozzle, re-homing the printer to redefine the home position was necessary after each adjustment. This also meant that the outcome of small adjustments could not be perceived in real time—rather, it was a system of constant trial-and-error in which the effect of a minute adjustment can only be evaluated after re-homing and bringing the nozzle back to a 0mm position. Furthermore, the circular bed plate was tensioned with three screws, each spaced 120° apart along the outside edge of the circle. It was not possible to change tension in exclusively an x- or y-direction, as the adjustment of one screw would affect the height of the print bed in adjacent regions as well due to the rigid nature of the bed plate.

Initial Printer Testing

Following assembly, the printer was first tested by bringing the printer to a home position, in which the hotend was fully raised to a $Z = 228$ mm position with each linear axis carriage activating its corresponding endstop at the top of the guide rail. However, this was initially unsuccessful, as two axis stepper motor gears were slipping on the timing belt and failed to cause movement. Attempts to further tighten the timing belts and lubricate the guide rail shafts were

eventually successful. It is important to note that the belts require retightening over time and that the shafts require frequent lubrication with lithium grease.

Initial printing of the printer post-assembly with the manufacturer-supplied STL object and polylactic acid (PLA) starter filament did not yield successful results. The printer and slicing/control software were configured according to the product manual [20], and the print was executed on the software side without significant issue. However, filament failed to enter the Bowden (PTFE) tubing after being propelled by the extruder motor. This was due to the filament end impacting the circumferential edge of the PTFE tube rather than entering the tube's hollow center. An effective fix for this issue involved using a scalpel to bevel the inner circumference of the tubing, thereby creating a funnel that would guide the filament into the tubing after coming out of the extruder motor. After resolution of this issue, PLA filament was fully inserted into all three hotend inlets to prevent the backflow of filament into unoccupied cold ends.

A second attempt to print a test object with PLA at 200°C did not yield successful results. Filament did not extrude freely from the heated nozzle, even with significant force applied by the extruder motors. Extrusion was limited to small drops of melted filament. Overheating the nozzle to further liquefy the filament did not result in a noticeable change in results. The issue, suspected to be a clogged hotend, was resolved after complete disassembly of the extruder. The cold-end cooling fins were removed from the hotend nozzle, and all visible filament residue was cleaned. Filament residue within the hotend itself was removed by heating the hotend to 230°C and pushing out the remains with a small-gauge screwdriver.

When fully reassembled, the hotend was able to more freely extrude PLA filament. However, the extrusion rate was still below an acceptable standard, and significant assistive manual driving forces were required to extrude filament, as the forces generated by the extruder motors

themselves were insufficient to propel the filament. This resulted in a major underextrusion issue.

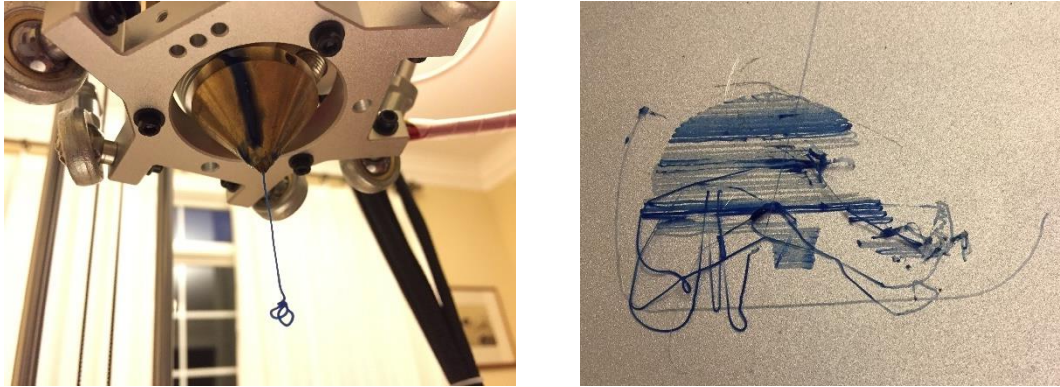


Figure 15. The hotend thinly extruded filament only after the application of manual pressure on the filament entering the extruder motor. The resulting failed print demonstrates insufficient material extrusion and adhesion.

At this point, the printer was functioning to its out-of-box potential. Further modifications would be needed to rectify inherent design issues and accommodate project specifications. These shortcomings and subsequent modifications are addressed in the following section.

4.2. Extruder Motor Modifications

In analyzing the underextrusion issue, the two major components involving extrusion were investigated. The first was the extruder motor, where the filament originates, and the second was the hotend, where the filament is received. This section describes the diagnosis and treatment of extruder motor issues, and the hotend will be discussed in the following section.

Under normal circumstances, the squeezing force of the extruder gear against the filament should cause the gear to bite into the filament. The turning of the gear then propels the filament forward. However, out of the box, the extruder motor failed to firmly bite into the filament hotend,

causing the gear teeth to “skip” on the filament surface after encountering only mild resistance. This was due to insufficient force applied by the toothed gear on the filament.

Higher-quality extruder frames typically bundled with extruder motors, such as the one depicted below, are tensionable with an adjustment screw. The tightening of the screw increases the force applied by the tension spring, which increases the inward force of the tension wheel against the filament. However, the extruder frames that arrived with the printer were made of non-tensionable plastic.

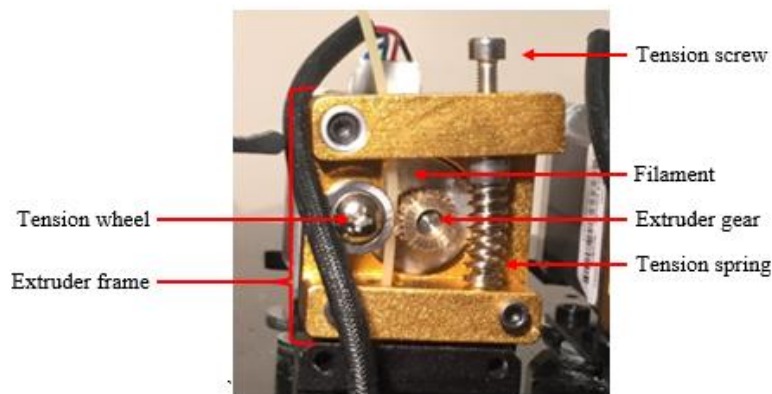


Figure 16. Typical high-quality metal extruder frame with labeled components. The filament is extruded by the turning of the extruder gear. Pressure on the filament can be increased by adjusting the tension screw, which compresses the tension spring and increases its exerted force. This force is translated to the tension wheel, which is driven inward towards the extruder gear.

To address this issue, the original low-quality plastic extruder frames were replaced by tensionable metal frames [21]. However, the replacement metal frames were not fully compatible with the original M8-sized Bowden tube pneumatic-style connectors, which connect the frame to the Bowden tube. The metal frames’ filament outlet only accommodated smaller, M6-sized Bowden connectors. As a temporary but imperfect fix due to budget constraints, the original Bowden interface assembly was wedged between the metal frame and the printer’s top plate.

This serves as an adapter, allowing filament to travel from the metal frame into the original assembly and eventually out of the original Bowden tube connector. This required extra space accommodation between the frame and the printer's top plate, and so the entire extruder motor itself was offset from the plate using four large washers. Future work should consider replacing this temporary workaround with a simple, proper-fitting MC6-sized Bowden connector directly on the metal frame.

Lastly, the filament skipping issue was addressed by increasing the voltage supplied to the extruder motor by adjusting the potentiometer on the stepper driver. The voltage was increased from 0.5V to 0.8V, after which the torque of the motor noticeably improved.

As a last measure to lower the resistance between the extruder motor and the hotend, the length of the Bowden (PTFE) tubing was shortened. Eliminating this excess length decreased the amount of friction between the filament and surrounding tubing, facilitating more effective extrusion.

4.3. Printhead Design Modifications

After modifications were made to the extruder motor, problems with filament extrusion from the hotend persisted. Very high amounts of force were required to push the filament into the hotend, and still relatively little molten filament came out of the nozzle. It was evident that the issue was not with the extruder motors—in fact, the high amounts of force and torque applied by the motor was causing the filament to be stripped. This indicated that the hotend was the next bottleneck.

Multiple attempts to overheat the hotend and unclog the chambers were unsuccessful. Abrasive cleaning filament [22] was also introduced into the hotend in attempts to remove stubborn particulate matter accumulated in the chamber. However, the cleaning filament was similarly

unable to extrude properly. These unclogging attempts should have resolved the problem if particulate obstruction were the issue. The Bowden tubes feeding filament into the hotends were inspected to ensure low resistance, complete and proper insertion, and clean/straight ends. Due to collective inability of these exhaustive steps to promote sufficient extrusion, an inherently poor build quality of the hotend was suspected. Investigations on online forums reveal that hotend issues with this printer are relatively common [23]. Phone conversations with the manufacturer yielded no new troubleshooting guidance.

One plausible diagnosis suggests that the internal chambers within the hotend (Fig. 17) are not smoothly drilled to the correct diameter. As a result, the molten filament encounters high resistance within the hotend. This issue is difficult to resolve due to the nature of the hotend as a precision instrument. Any manual retooling has a high risk of rendering the entire hotend unusable.

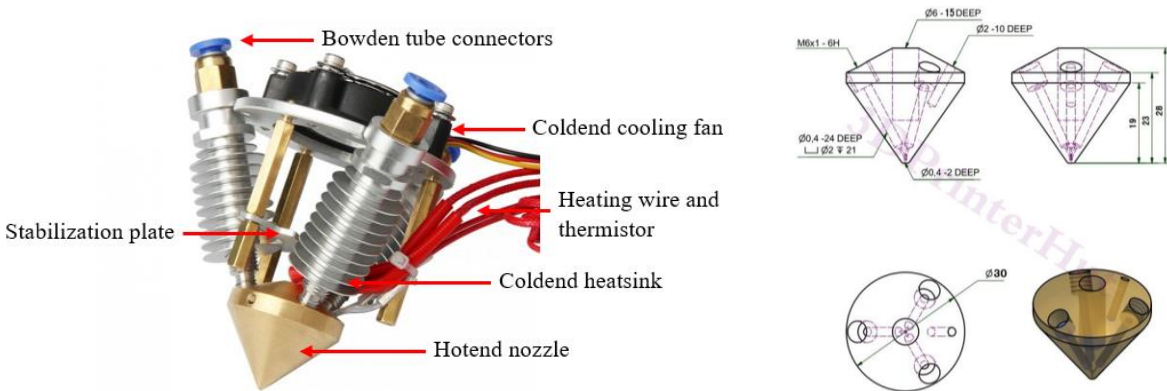


Figure 17. Left: Original mixing hotend of the Geeetech Delta Rostock 301 3D printer. Right: Internal nozzle configuration of the Diamond Hotend, off which the Geeetech nozzle is based. Image: Aliexpress [35]

Ultimately, it was decided that the inexpensive, low-quality hotend—which is a generic clone of the well-known Diamond-brand hotend—should be replaced in its entirety by its higher-quality

counterpart. Though the genuine Diamond hotend would result in an additional \$60 expense, the mission-critical nature of this component factored heavily in the cost-benefit analysis.

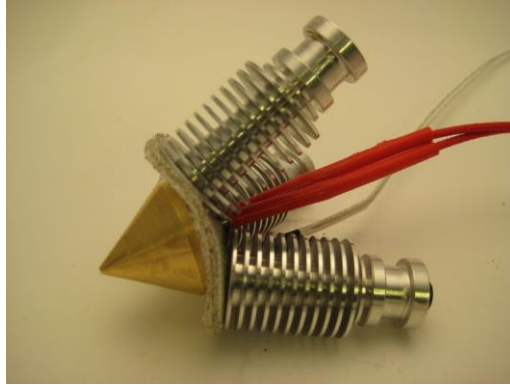


Figure 18. Genuine Diamond hotend. Nozzle, heatsinks, heating element, thermistor, and insulation between hotend and coldend assembled. Image: RepRap.me [30]

The genuine Diamond hotend, with attached cooling fins, is slightly larger than the lower-quality clone it replaced (Fig. 18). As a result, modifications to the hotend mount and carriage assembly were required for the proper mounting of the Diamond hotend. Specifically, the metal stabilization plate that provided additional reinforcement between the heatsink and the carriage mount was removed due to its improper size. Instead, the entire Diamond hotend assembly was secured to the carriage directly with only the original top metal frame, which pressed the hotend assembly against the bottom of the carriage with the original tension screws (Fig. 19).

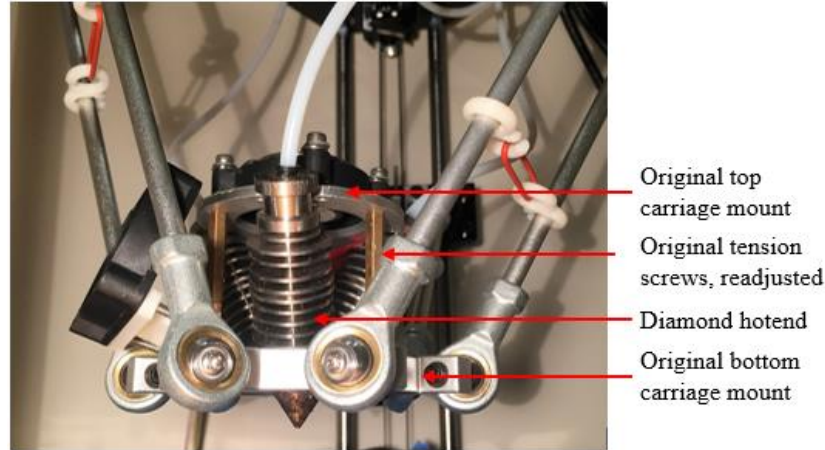


Figure 19. Mounting of genuine Diamond hotend assembly. New assembly is secured between top plate and bottom of carriage using tension screws.

The thermistor and heating element supplied with the Diamond hotend were used in lieu of the original components and reconnected to the printer's electronics accordingly with minor connector modifications.

Following the installation of the Diamond hotend, manual extrusion was successful. The hotend temperature was successfully raised to 200°C, and Repetier-Host control software was used to manually extrude filament from the nozzle. The filament flowed freely with minimal resistance, in sharp contrast to the singular occasional drips that emerged from the original hotend.

4.4. Test Prints and Analysis of Non-Rotated Blocks

Testing and Analysis of Build Phase 1 Blocks

After the successful extrusion of PLA, a test object from an STL file provided by the manufacturer was sliced and printed. This was performed using Slic3r and Repetier-Host according to the manufacturer's default printing recommendations [20]. The first few printing attempts failed due to first layer adhesion issues, in which the molten filament would not adhere

to the build plate. To address this issue, the build plate was recalibrated and covered with blue painter's tape—a common technique to increase the friction of the build plate. This rough, uneven surface provided more microscopic attachment points to which the filament can attach and adhere, resulting in the first successful print.

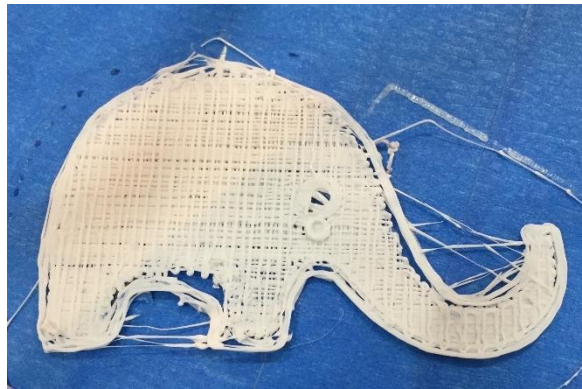


Figure 20. First PLA object printed by the modified 3D printer. Though print quality is low, successful extrusion and the ability to form actual prints are critical first steps.

Further testing was conducted by printing 1-inch PLA blocks to gauge dimension tolerancing and infill quality. Three 1in. \times 1in. \times 0.5in. blocks were printed; their dimensions were measured and the results are reproduced in the table below.



Figure 21. Testing of Phase 1 test print dimensions and tolerances.

	Length	Width	Height
Block 1	1.0110 in.	1.0000 in.	0.5220 in.
Block 2	0.9965 in.	1.0040 in.	0.5105 in.
Block 3	1.0210 in.	1.0025 in.	0.5170 in.
Average Deviation	0.0095 in.	0.0022 in.	0.0165 in.

Table 3. Dimensions of Build Phase 1 test blocks. Theoretical dimensions: 1 in. x 1 in. x 0.5 in.

Analysis of these data reveals that the printer is, on average, capable of producing objects $1\text{in.} \pm 1\text{-}2\%$ along the lengths and widths of the blocks. The printed height is slightly less accurate, with measurements in the $0.5\text{in.} \pm 2\text{-}4\%$ range. The most recent phantom design, in which cubes are placed in a $3 \times 3 \times 3$ pattern, does not require that each block be extremely precise. Large spaces are present between blocks, so they need not be assembled; furthermore, small variances in size should not impact the diffusive properties of the material within the block itself.

Test Printing of Build Phase 2 & Build Phase 3 Blocks

Following the printing of a PLA object, the build proceeded to Build Phase 2 with the single-extrusion of Lay-felt and Gel-lay. Despite prior success within the group of printing Gel-lay blocks on a Prusa i3 printer, similar success was not found with attempts to print with Lay-felt. The first step involved replicating the success of printing Gel-lay, which was achieved after removing the original PLA filament, cleaning the nozzle with cleaning filament, and inserting Gel-lay in all chambers.

Manual extrusion of the Gel-lay was successfully performed at 225°C , within the manufacturer’s specified range of $225^{\circ}\text{C} - 235^{\circ}\text{C}$. STL designs of square cubes were then made in SolidWorks and imported into slicing software. The blocks were sliced according to the settings outlined in Chapter 5 of this report, and instructions were sent to the printer for printing.

Printing test cubes with the Gel-lay was generally successful. As an immediate next step, the Gel-lay was replaced with Lay-felt, and the process was successfully repeated with the printing of a non-rotated, 100% Lay-felt block. This importantly demonstrated the printer's ability to extrude our nonconventional materials.

Development quickly shifted into Build Phase 3, in which mixed extrusion of the two materials was attempted. The printer was first prepared by placing Lay-felt in Extruder 0, Gel-lay in Extruder 1, and PLA in Extruder 2. Upon proper configuration, the extruder motors for Lay-felt and Gel-lay successfully propelled both filaments into the hotend simultaneously, resulting in mixing and dual extrusion. On the software front, this was performed by initiating a standard single-extrusion print, similar to Build Phase 2, and then manually configuring the mixing ratio on the printer interface according to the desired ratio.

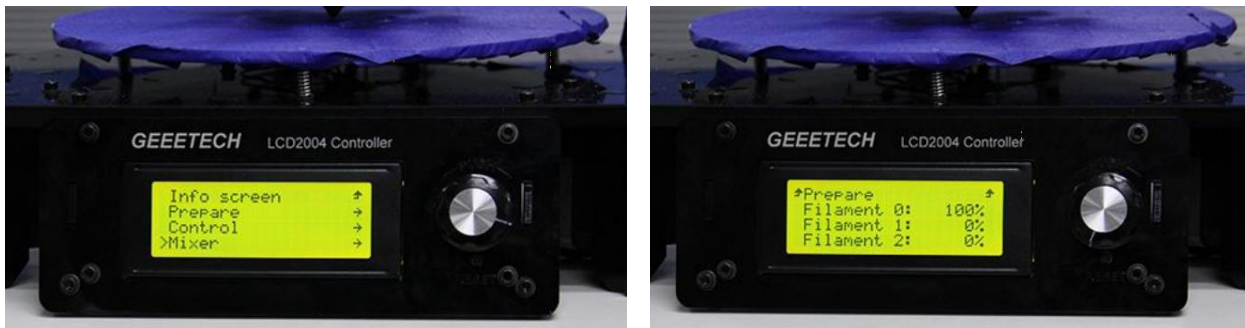


Figure 22. Initial configuration of mixed-block printing using the printer interface. The ratios of Lay-felt and Gel-lay can be adjusted by entering the Mixer menu (left), in which the desired percentages of each filament can be specified (right).

The successful extrusion of a Gel-lay/Lay-felt mix was a crucial step in the build process, as it demonstrated the feasibility for these two non-conventional materials to mix in a stable way and produce a structurally sound and homogenous print (Fig. 23).

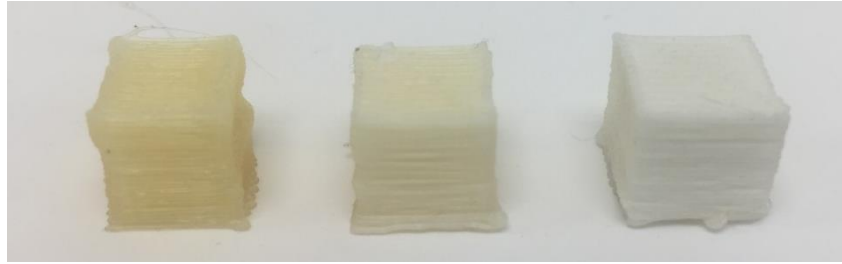


Figure 23. 100% Gel-lay cube (right), 50% Gel-lay/50% Lay-felt cube (middle), and 100% Lay-felt cube, printed during Build Phase 1 & 2 testing. Note the variations in color based on material: Gel-lay is yellow in color, while Lay-felt is white. As expected, the mixed extrusion product is a white-yellow.

Analysis of Build Phase 2 & Build Phase 3 Blocks

Analysis of the first prints revealed several quality issues. Most notably, rather than having flat sides, the cubes exhibited warped, wave-like behavior on two faces. These two faces were the ones comprised of the ends of infill tool paths, where a 180° direction change of the print nozzle occurred. The non-linear behavior exhibited on these faces was primarily due to the sudden reversal in carriage direction, which acted in opposition to inertial forces, causing erratic print behavior.

These conflicting forces resulted in significant wobble of the printer chassis—an issue exacerbated by the high frequency of direction changes. Combined with the printer’s height and lack of stabilizing cross-beams, the printer was extremely unstable in the x-y plane. In fact, one of this printer’s critical design flaws includes using the axis guide rails simultaneously as structural support beams. As such, no other structural supports exist to counteract the forces propagated from the rails. In its original form, this printer would only be capable of producing larger parts requiring far less precision, and at much lower speeds.

4.5. Chassis and Stability Modifications

In response to the analysis of blocks from Build Phases 2 and 3, printer stability modifications were needed. To modify the design of the printer to minimize wobble, several ideas were considered. The first involved utilizing T-slots to build an external frame for the printer. The T-slots would act much like cross-beams on a building, providing structural rigidity by limiting movement in the x-y plane. Another option involved securing one side of a printer to a board, which would act as a rigid backbone for the printer. These two options, however, would be difficult to implement given the awkward shape of the printer. Furthermore, the printer does not have many mounting or attachment points for additional hardware, which would require the T-slot or board backbone designs to contain an intricate attachment mechanism. The complexity of design required, combined with the unsightly nature of additional bulky hardware, decreased the preference of these two options.

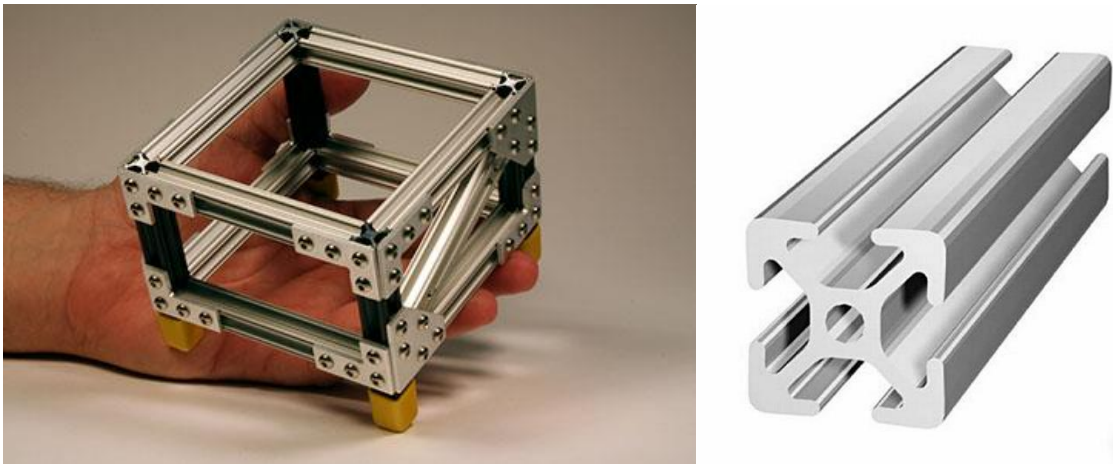


Figure 24. Small-scale example of a T-slot frame (left) and a close-up view of a T-slot beam (right). Aluminum T-slots are lightweight and resist deformation, though are often difficult to assemble around irregularly-sized objects due to their linear shape. *Images: Corecommerce, Singcore [31, 32]*

A third option included shortening the height of the printer. Wobble happens most severely at the highest point of the structure, while stability is maximized at the bottom. By this notion, the printer is akin to an oscillating lever arm fixed at one end at the printer-table interface—in which the friction force between the printer and the unmovable table acts as a fulcrum. The moment of inertia of such a lever arm is $\frac{1}{3} ML^2$. Effectively, halving the height of the printer would decrease the moment of inertia by a factor of 4. Wobble, described by angular momentum, is directly proportional to the moment of inertia. Thus, any reduction in height would appreciably decrease the effect of sudden carriage path reversals on wobble. Ultimately, this design option was selected due to its effectiveness, accessibility, and relative ease of implementation.

Printer Shortening Design

Six steel rods, acting both as linear guide shafts for the carriage bearings as well as structural support beams, are connected to the top and bottom plates of the printer. The rods are stepped down to a slightly smaller diameter on the ends to fit into corresponding holes on the top and bottom plates. Screws on either end of the rods secure the base-plate/rod/top-plate assembly, which requires that the rod ends be tapped.

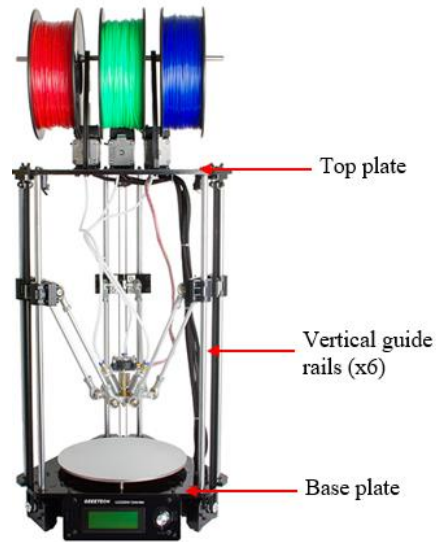


Figure 25. Printer height is determined by the lengths of the six vertical guide rails. The reduced-diameter ends of the rail fit into holes on the base and top plates. Screws on either end secure the rails to the plates.

The modified height of the printer was informed directly by the height of the cubes. Because the cube is 1 cm tall, it was determined that a total print height of 3 cm would be appropriate, minimizing unused overhead room without compromising a full range of motion. Based on this value, it was determined that the new vertical connecting rods needed to be 30 cm, or 11.8 inches. Conveniently, steel rods are sold at a 1-foot standard length from McMaster-Carr, the Group’s preferred hardware vendor.

Selection of the new rods was based on the following specifications:

Dimension	Value
Total length	30 cm (11.8 in.)
Major (shaft) diameter	10 mm
Minor (stepped-down) diameter	8 mm
Step-down length	8 mm
Tap size	M4 X0.7 D2

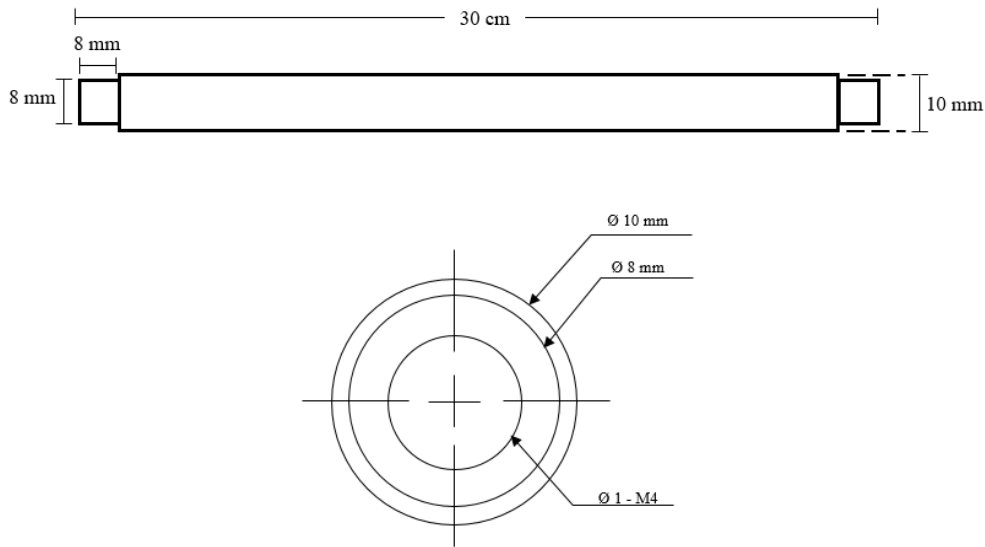


Table 4 and Figure 26. Shortened rod specifications.
Side-on view (top), end-on view (bottom). Images not to scale.

Two options for rod sourcing were considered. One option was to cut and re-machine the existing rods, while the other was to purchase new rods. It was decided that purchasing new rods, while keeping the existing ones intact, would be the more conservative and prudent measure. This would ensure that the printer is still usable in the event that shortening is unsuccessful or if restoration to full height is needed in the future.

Because of budget limitations, the cost of the new rods was a primary consideration. Custom-ordering rods with the above specifications would yield costs in the \$100+ range. Instead, generic steel rods were purchased, with the expectation that they would need to be self-machined. After considerations of material, machinability, and manufacturing technique, it was decided that the McMaster-Carr 12L14 Carbon Steel Metric High-Tolerance Rod [24] would be most suitable. The 12L14 rod is made of leaded, annealed carbon steel, allowing for high machinability while maintaining sufficient strength, hardness, and straightness tolerances.

Machining was performed with a Wabeco D6000 manual lathe in the Simulation Group labs after basic training. The one-foot rods were first taken down to an overall length of 30 cm. Afterwards, the diameter of each end was reduced to 8 mm from the overall shaft diameter of 10 mm. This stepped-down region measured 8 mm in length on each end, allowing for $30 \text{ cm} - 2 \times (8 \text{ mm}) = 28.4 \text{ cm}$ of the original 10 mm diameter shaft remaining the middle.

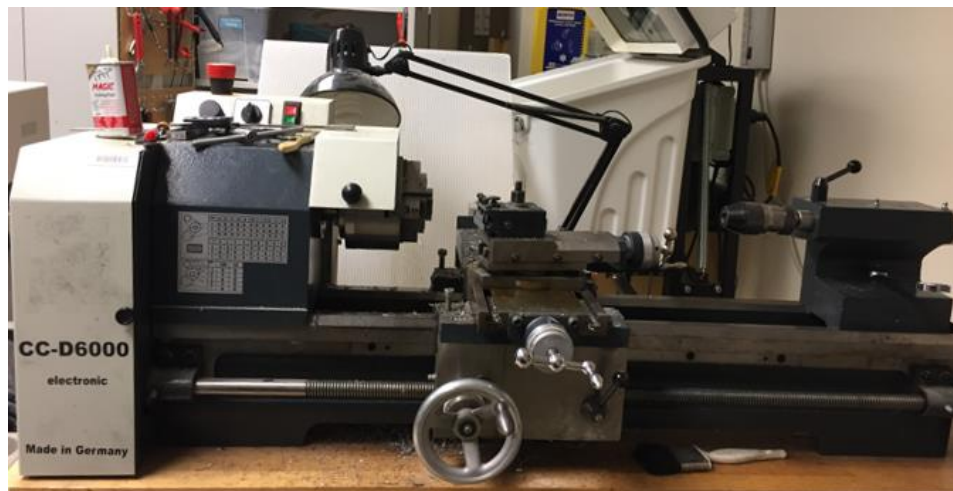


Figure 27. Wabeco CC-D6000 lathe used in machining new guide rail rods.

Afterwards, each end of the six rods were tapped. A lathe-mounted #30 drill bit was used to create tap holes approx. 2 cm deep. After lubrication, a standard M4 X 0.7 D2 tap was used to thread the hole, corresponding to the original screws used to secure the rods in place.

Following the machining process, the new rods were installed. Rod ends were inserted into the bed plate holes with the original washer placed in between. The z-axis print height was ultimately 31 mm, closely corresponding to the original design goal. With manual modification of the printer firmware done through the printer's LCD screen, the new printer height was set as 31 mm and subsequently re-calibrated.

Testing the shortened printer with newly printed blocks revealed much higher print quality. Compared to old blocks, new ones exhibited significantly flatter faces, straighter edges and infill lines, and less oscillatory behavior at block corners.

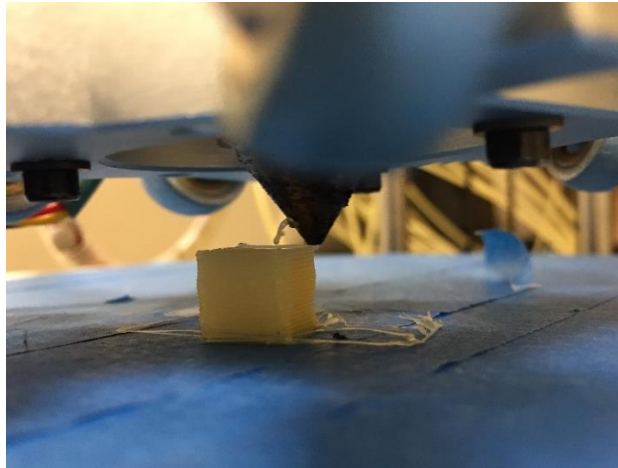


Figure 28. Testing of block printing post-shortening. Block edges and faces are noticeably flatter, though minor deficiencies still exist.

Carriage Arm Tensioners and Belt Tensioners

From further observation of the printer during operation, it was also observed that the carriage arm ball-and-socket joints connecting the carriage arms to the carriage mount were poorly fitted. This decreases the responsiveness of the hotend mount to carriage arm movements, while also contributing to unwanted wobble. To enhance the design, S-shaped rod clips were printed from Thingiverse [25], attached to the carriage arms, and tensioned with O-rings (Fig. 28). This pulls each pair of carriage arms towards each other, reducing residual movement in lateral directions.

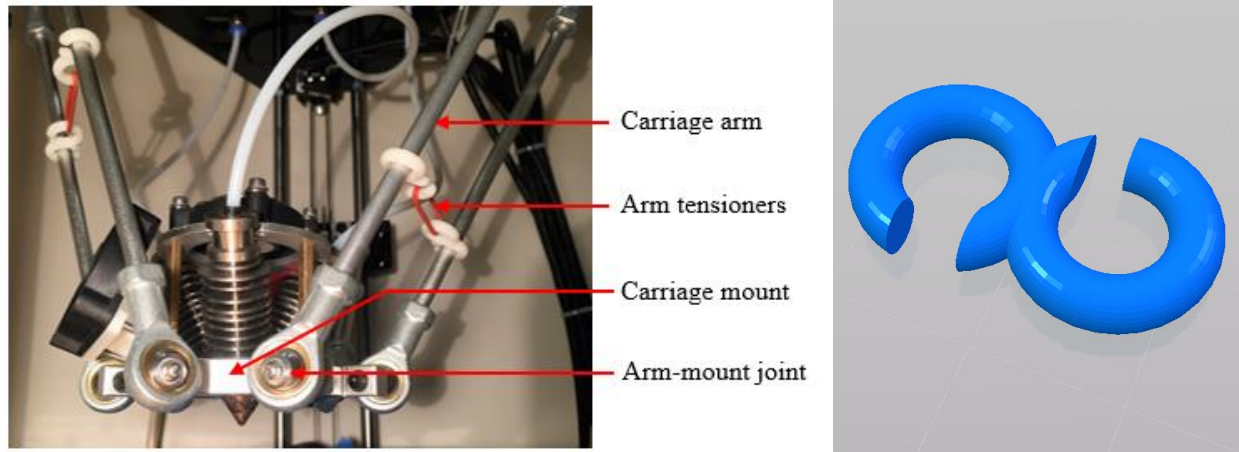


Figure 29. CAD rendering of the S-shaped rod hook (left) and implementation on the printer (right). When tensioned by a small O-ring, lateral arm movement is restricted, reducing unwanted wobble.

Additionally, to increase the sensitivity of the carriage arms in response to axis motor movements, the belts were further tensioned. To allow for more dynamic tightening in the future, the short tensioning screws connecting the top plate to the belt pulley assembly were replaced with longer screws. The longer screw ensures a greater tightening range, allowing for minor adjustments over time as the belt deforms.

4.6. Build Plate Fans

During the printing of blocks in Build Phases 2 and 3, it was evident that many layer edges were also not well-defined due to the dragging of newly printed filament. Without a build plate fan (i.e. layer fan), newly extruded filament remains soft due to retained heat, resulting in poor fusion with the preceding layer. This unanchored material is then easily pulled in the next direction of nozzle movement. Additionally, in the middle of the layers, the warping of soft filament can occur due to the pressure exerted by subsequent filament lines and layers. This

behavior is seen in the block below, where deformation of molten filament in one layer causes failure in all subsequent layers.

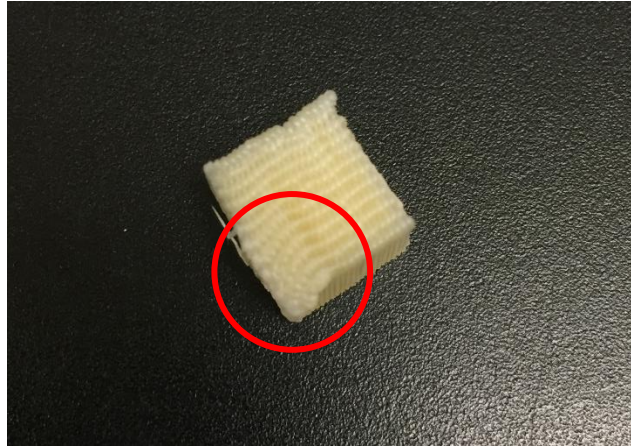


Figure 30. Warping behavior at block edge due to dragging behavior and heat accumulation. Defects in one layer impact all subsequent layers.

To ensure that new filament hardens in the proper position as soon as it is extruded, bed plate fans were installed. These fans, directed at the printed piece, are designed to rapidly cool down newly extruded material by introducing cooler ambient air. Two bed plate fans were added, allowing the persistent introduction of cool air to the part. One standard 40 mm × 40 mm × 15 mm box fan was attached to the print carriage using a 3D-printed ABS mount, whose design was sourced from Thingiverse [26]. In addition, a 50mm radial fan was secured to the edge of the bed plate itself using two-sided foam tape. This fan, located opposite from the other 40mm box fan, is particularly effective at introducing a constant powerful stream of cool air to the part. Its small duct opening matches the small geometry of the block, allowing for high surface area contact. Working together, substantial airflow was channeled to the part.

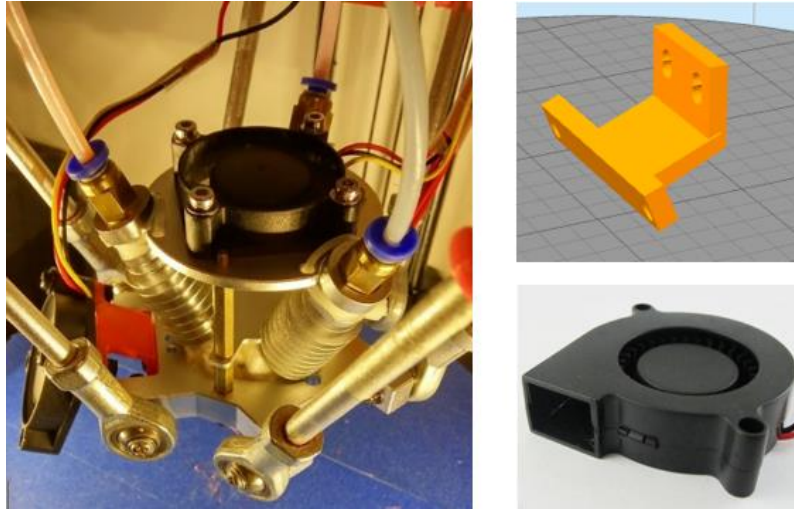


Figure 31. A 40mm bed plate fan was secured to the carriage (left) with a 3D-printed mount (right, top). A 50mm radial blower fan is placed on the other side of the build plate to introduce cool air from the opposite direction. *Images: Thingiverse, Aus3D [26, 33]*

Other more complex designs were also considered, such as carriage-mounted ring ducting to provide symmetric cooling on all sides. However, despite the likely marginal benefit of more robust ducting, no existing designs were found that would properly fit the printer carriage. Thus, implementation would require significant original CAD work, which would require further training and the expensive consumption of time resources. As such, the easier—but sufficiently effective—design with two disjoint fans was implemented.

After replacement of the bed fan, a noticeable decrease in the frequency and magnitude of block warping behavior was observed.

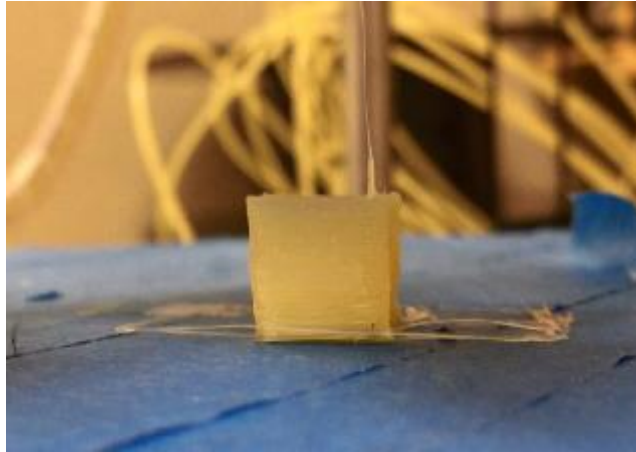


Figure 32. Block printed after installation of build plate fan. Blocks printed with active cooling from the bed plate fans exhibit flatter faces and straighter edges without substantial warping behavior.

4.7. Driver Board Replacement

After the testing of non-rotated single- and mixed-extrusion blocks, Build Phase 4 began with the single-extrusion of rotated blocks. Implementation of Build Phase 4 was mostly software-based, as all relevant hardware designs have already been properly configured. Thus, a discussion of Build Phase 4 will be discussed in Chapter 5.

The progression from Build Phase 4 to Build Phase 5, however, required significant hardware changes. In Build Phase 4, mixed extrusion was initially achieved by setting the mixing ratio via the printer LCD interface per the manufacturer’s guidelines. This was done by first sending a standard, single-extrusion G-code script to the printer. The filament ratio was then manually configured by entering the “Mixer” configuration on the printer interface. This is referred to as firmware-based mixing. However, to allow for mixed extrusion on a larger scale, G-code based mixing is necessary. This would allow mixing commands to directly be incorporated into the G-

code, delivering automated mixing commands to the printer without the need for manual controls before each print.

Furthermore, the printing of rotated cubes with mixed materials and support structures in Build Phase 5 also requires G-code based mixing. This is because tool change commands (needed to switch between support material and print material) would reset any manual firmware-based mixing settings on the printer interface. While manually configuring the mixing ratio is possible when no tool changes occur (in the case of non-rotated cubes), this practice becomes practically impossible when the settings are reset every layer.

The native printer firmware packaged with the Geeetech GTM32 Pro controller board does not support G-code based mixing. In addition, the 3D printer's driver board is closed-source, which prevents any consumer-end modifications to the firmware. This prohibits the printing of rotated, mixed cubes of any kind. In contrast, industry standard firmware, such Marlin or Repetier, both support G-code based mixing as of most recent versions.

Installation of RUMBA Controller Board

As a result of these software limitations, the printer's driver board was completely replaced with a new RUMBA board. A RUMBA board was selected because of its versatility, supporting multiple types of open-source firmware—including both Marlin and Repetier, which permit G-code-based mixing. The board also has connectors for three extruder stepper motors.

Additionally, the group's Dr. Galanaud owned a spare RUMBA board, which was borrowed for testing purposes.

This completely proprietary board hardware also had unconventional electronics, and thus significant modification of the printer wiring was needed. New mounting holes were first drilled

at the bottom of the printer's base plate to accommodate the new board's larger geometry. Once secured, rewiring was performed in the ways described below. A labeled diagram of the board is provided for reference.

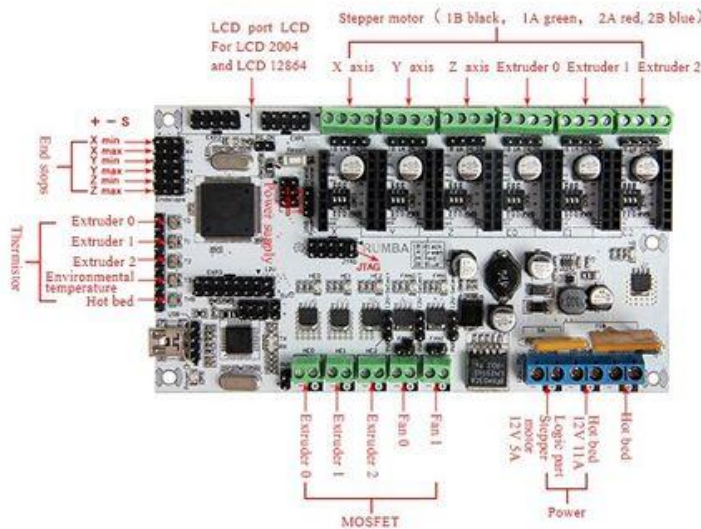


Figure 33. Standard RUMBA controller board with labeled connectors. *Image: RepRap.org [34]*

1. Direct wiring of extruder stepper motors to the controller

Originally, the extruder stepper motors were wired to a small integrated circuit (IC) mounted above each stepper motor, and a secondary, proprietary cable then ran from the ICs to the controller board. The small IC also had connectors for the hotend, thermistor, hotend fan, and extruder motor fan. This allowed all wires from the hotend assembly to run upwards, connect to the extruder motor-mounted IC, and then run down to the controller board in one integrated cable. While this complex configuration was appropriate to minimize wire clutter in a taller printer, the shortened printer was less susceptible to excessive wire length. Furthermore, this type of proprietary wire configuration was also not supported by the new RUMBA board.

In the new configuration, industry-standard 4-pin extruder motor wires connected the motors directly to the axis stepper motor pins on new controller board. The proprietary ICs were therefore not needed and subsequently removed. Following the removal ICs, the extruder motor fans no longer had a neighboring connector. Due to their insignificant cooling role, they were subsequently removed.

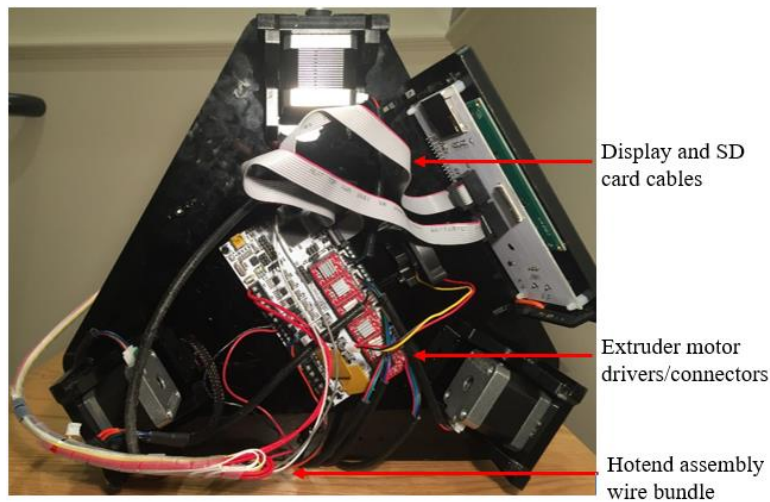


Figure 34. Printer electronics following installation of RUMBA controller board.

2. Direct connection of hotend assembly wires to controller board

With the removal of the extruder motor-mounted ICs, the hotend assembly wires—consisting of the heating element, thermistor, hotend fan, and carriage-mounted bed plate fan wires—were directly connected to the controller board beneath the printer. To ensure the cables do not interfere with the motion of the carriage during printing, they were partially suspended above the printer carriage with a zip-tie before being routed downwards. The bare hotend wires were connected to Extruder 0, while the bare thermistor wires were soldered onto jumper cables for connection to the Extruder 0 Temp pins. The hotend fan was connected to the Fan 0 wire clamp

connectors, while the carriage-mounted build plate fan was connected to the Fan 1 wire clamp connectors. The build plate-mounted 50mm radial blower fan was connected to the Fan 1 pin connectors.

3. Endstops and axis stepper motors

All endstop wires were removed from their proprietary multi-pin housings with the metal crimp portions still intact. These crimped female connectors were then wrapped with insulating tape and directly connected to the corresponding X-, Y-, or Z- MAX connectors on the (-) and (S) pins. As endstops are simply switches, wire order does not matter.

Axis stepper motor wires were similarly removed from their joint proprietary housing (Fig. 35). The loose ends of each individual motor cable were then placed into a standard 4-pin housing with the wire order preserved. The standard 4-pin housings were obtained from the disassembly of the short extruder stepper motor cables that formerly connected the extruder motors to the small ICs. This allowed each individual axis motor to connect to the corresponding pins on the RUMBA board (X axis, Y axis, and Z axis).

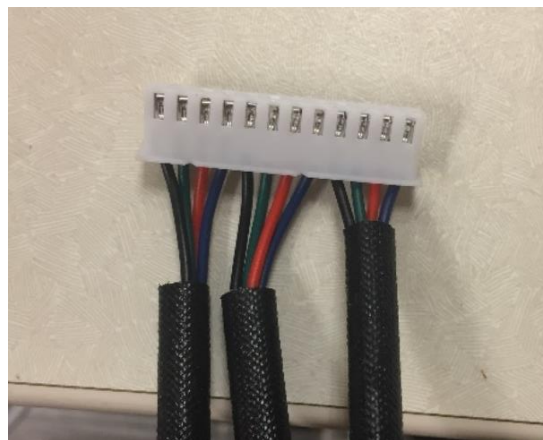


Figure 35. The three axis stepper motor cables originally attached to an integrated, proprietary housing. They were subsequently separated into three different 4-pin standard housings.

4. Power, display, and build plate

The original Geeetech power supply employed a socket connector, while the RUMBA board only accommodates bare wire. Thus, a standard 12-volt computer power supply, formerly used for the lab's Prusa i3 printer, was used for the new board.

The original thin ribbon cable connecting the printer's LCD 2004 connector was replaced with a standard 10-pin LCD and SD card bus cable. These cables directly connected the display and SD controller to the EXP 1 and EXP 2 pins, respectively. The heated build plate is not necessary for Lay-felt, Gel-lay, or PVA, and so it is not connected.

Testing of New Controller Board

After hardware configurations were complete, new firmware was uploaded as described in Section 5. Initial tests involved sending G-code scripts containing mixed extrusion commands and verifying the movement of multiple extruder motors at once. Afterwards, more detailed testing was done to ensure that the printer was physically extruding the proper amounts of filament in response to G-code commands.

This test was conducted by measuring the length of filament consumed by prints of various ratios. Graduations of 5 mm were made in permanent marker along the filament to be fed into the extruder motor. Length of filament is used as a proxy for volume, as the filament diameters are of the same 1.75mm standard. If mixing is performed properly, then a 100mm extrusion of a 50/50 filament mix should consume 50mm of both Gel-lay and Lay-felt.

Test extrusions of 100/0, 50/50, and 0/100 Lay-felt/Gel-lay ratios were run. In the 100/0 and 0/100 tests, a command to extrude 100mm of filament resulted in the consumption of approximately 96mm of the corresponding filament. In the 50/50 test, approximately 48mm of

each filament was consumed by the two extruders. This demonstrates that the software-based mixing commands execute in the proper way; however, there is a calibration issue involving the firmware's `steps_per_mm` setting, as systematic underextrusion is occurring across the board.

While the installation of the new controller board and firmware was successful, the printing of actual rotated mixed cubes with support structures was not attempted before the conclusion of the project. This remains as an immediate next step for the project.

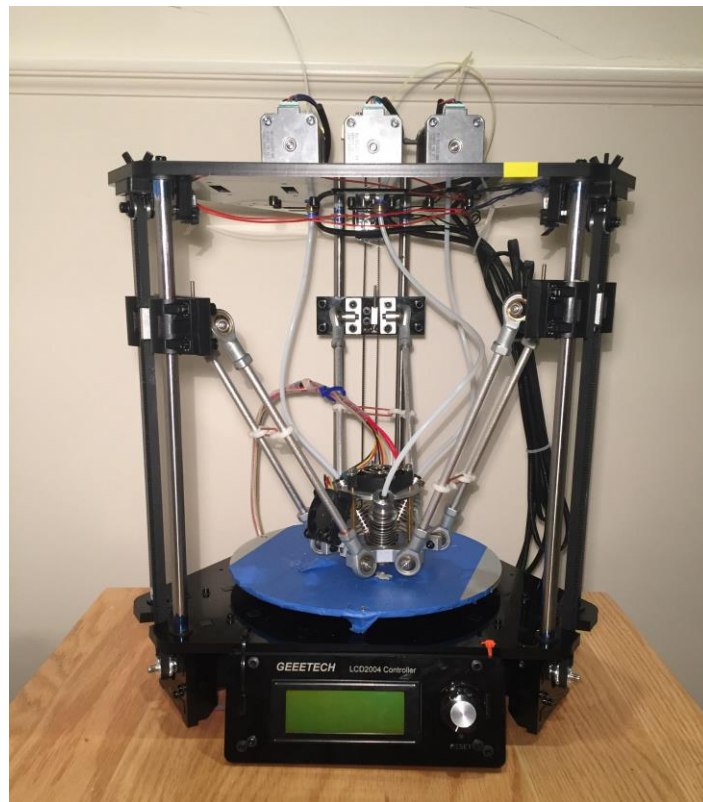


Figure 36. Fully assembled, modified 3D printer.

5 Software Settings and Evolution

Following the software selection process described in Section 3.3, each component required separate configuration. Overall, software configuration was a time-intensive process involving informed trial-and-error processes. Due to the use of nonconventional materials, the custom nature of the 3D printer, and the unique demands of this project, no established software settings exist. Instead, the software design process must begin from scratch with a best estimate of certain parameters based on best practices and generalizations. From that point, each variable must be adjusted and tested one-by-one to ascertain the optimal setting. Testing itself is an extremely time-consuming process, as each block takes approximately 10-15 minutes to print. Eventually, dozens of software settings were adjusted and refined to suit the unprecedented nature of this project, and the final configurations and design details are described in this chapter.

Although the process begins with the generation of 1cm^3 blocks within SolidWorks, this is a relatively simple exercise and will not be described here.

5.1. Slicing Software & Generation of G-Code

Simplify3D must first be configured for the customized 3D printer. Conveniently, within Simplify3D, the Configuration Assistant can configure most connection, geometry, and extruder settings automatically once “Geetech Rostock 301” is selected. The only adjustment involves redefining the printer height from 230mm to 31mm in the General Options window.

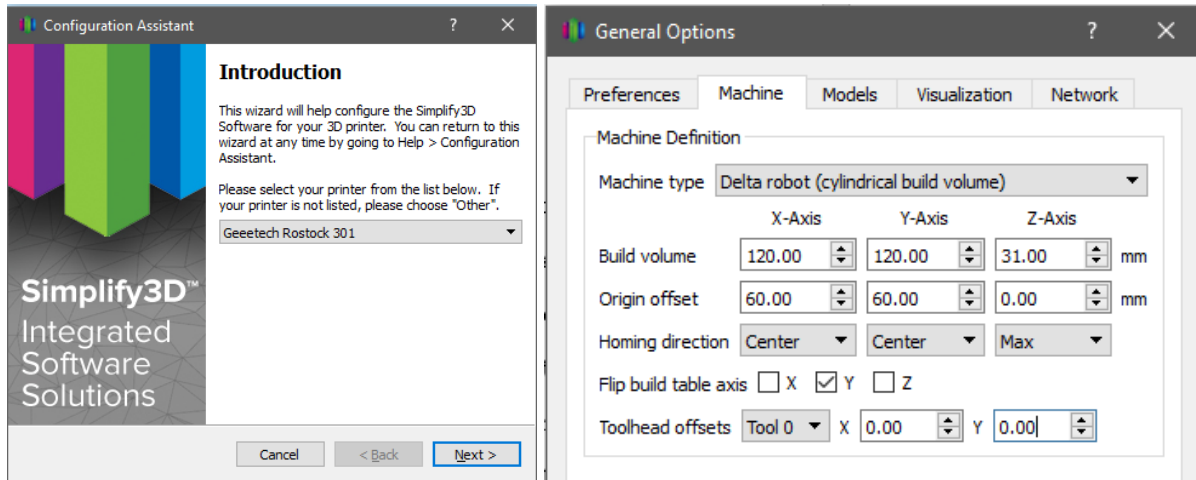


Figure 37. The Configuration Assistant (left) allows for easy configuration of Simplify3D. Only the Z-axis build height needs to be changed to reflect the new height of 31 mm (right).

Several settings are common across all blocks, no matter the material ratio or orientation. Blocks are printed with an 80% linear infill pattern density and zero outside perimeters. The hotend is set to 225°C without a heated bed plate, and the maximum speed is 60 mm/s to maintain quality during the print. Layer heights are 0.4 mm, consistent with nozzle diameter, and three skirts are printed before the part begins to prime the nozzle and promote adhesion.

Non-Rotated Cube Print Settings

After a STL file of a non-rotated 1cm³ block was imported into Simplify3D, G-code for non-rotated cubes was generated using the settings found in Appendix 12.1. Most notably, the cubes were made with an 80% linear-pattern infill density with zero outside perimeters at a speed of 60 mm/s. Filament was extruded at a temperature of 230°C with a layer height of 0.4 mm.

By default, the slicing software generates linear infill patterns that alternate in direction every layer, creating a woven pattern when multiple layers are overlaid. While this provides excellent mechanical stability, it does not permit diffusion, as perpendicular fibers obstruct the movement

of water. Thus, post-processing is necessary to align all tracts such that they face the same direction. This can be done by copying the G-code for the third layer and pasting this code for every layer from the second to the last. This ensures all layers are identical with lines in the same direction (Fig. 38).

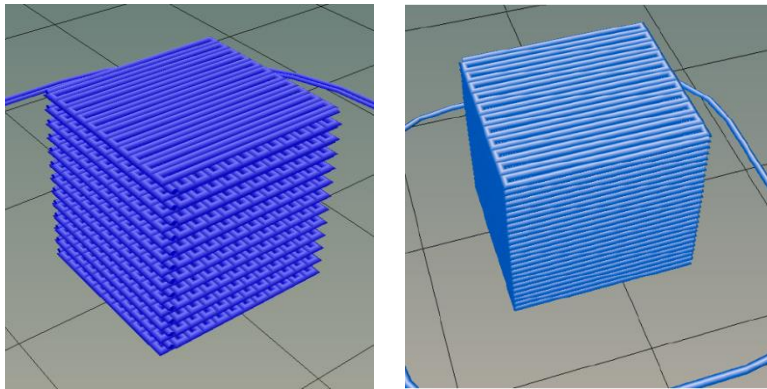


Figure 38. Non-rotated cube sliced with normal rectilinear infills without post-processing, exhibiting interwoven layers (left). During post-processing, perpendicular layers are replaced with parallel layers, resulting in completely parallel infill lines (right).

5.2. Rotated Cube Print Settings

Infill Lines

The printing of rotated cubes is a more complex process, as it involves the design and printing of support material. When the rotated cube is printed with only one corner in contact with the build plate, support structures must be constructed on all sides. In order to maintain the edge integrity of the phantom blocks, the support structures must also be appropriately dense.

After G-code generation, post-processing must occur to align all layers in the same direction. However, due to the rotated nature of the block, layers are not identical, and so the copy-paste method used for the non-rotated blocks would not work. As a workaround, the rotated cube was stretched vertically in SolidWorks by a factor of 2. After G-code generation, the deletion of

every other layer would eliminate perpendicular infill lines while simultaneously restoring the cube to its intended height. This necessitates a two-part process: 1) manually opening the G-code file and delete every other layer, starting at layer 2, and 2) changing all Z-coordinates of all layers such that they correspond to adjacent layers. While this was done manually, further opportunities involve automation of this process.

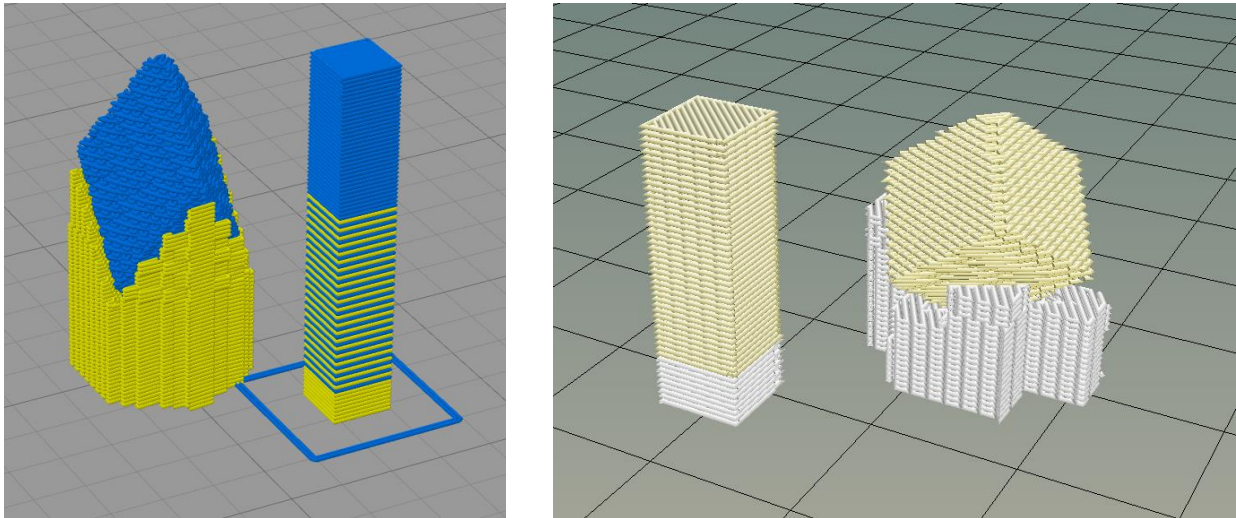


Figure 39. Vertically stretched rotated cube before post-processing (left). After removal of perpendicular layers, the proper cube height is restored.

Support Structure

Support structures were configured such that the maximum amount of support material was present on each side. This was achieved by changing the maximum overhang angle and support pillar resolutions to low values, such as 5 degrees and 1 mm, respectively. Test prints with less than 50% of the cube height supported by PVA exhibited sagging on the edges. Because the support is water-soluble, the horizontal offset from the part can be configured to 0mm.

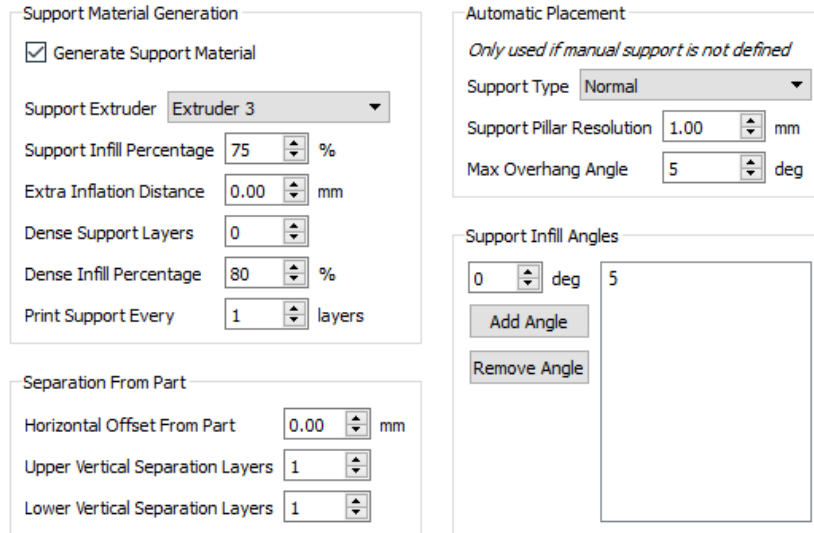


Figure 40. Support material print settings.

Priming Pillar

The priming pillar is a 3D-printed structure located directly adjacent to the rotated cube assembly. Its purpose is to serve as an extrudate discard area between filament changes. Without a priming pillar, filament changes would result in old material, such as PVA, mixing with new filament, such as Lay-felt, in the hotend chamber. This would result in an unwanted mixture being extruded to print the blocks or support material, which is undesirable.

Instead, this unwanted mix of filaments is used to print a priming pillar, which is later discarded. The priming pillar “primes” the hotend by flushing out old filament and filling it with new filament, ensuring pure extrusion of the intended material. Because the priming pillar is wasted material, best practice is to keep its size to a minimum while still ensuring all unwanted material is captured.

The below settings were used to define the properties of the priming pillar. A pillar width of 6mm ensures adequate purging without excessive material waste, while a speed multiplier of 130% increases the speed without jeopardizing the structural integrity of the block itself.

Interestingly, the software includes the priming pillar even after all tool changes have been performed. In our case, support material is no longer needed after the block gets halfway printed, since no more overhanging structures exist. However, the printer will continue printing a priming pillar, consuming both time and material. In future work, the best practice would be the removal of these lines corresponding to unneeded priming pillar layers.

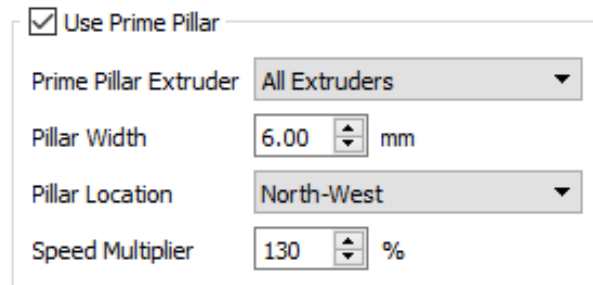


Figure 41. Prime pillar settings

5.3. Printing and Testing of Rotated, Single-Extrusion Blocks

Following software configuration of the support material and priming pillar, single-extrusion rotated cubes were printed for analysis. The printer successfully integrated the settings for the priming pillar and mid-layer tool changes, ensuring purity in the block material. After printing was complete, the priming pillar was cut off by hand, while the rest of the block print was submerged in water to remove the soluble PVA support material.

Although the prints demonstrated the printer's capability of producing support structures, significant amounts of oozing behavior were also observed. Oozing occurs when excess material accumulates at the ends of travel moves, resulting in blobbing behavior or filament stringing during travel moves.

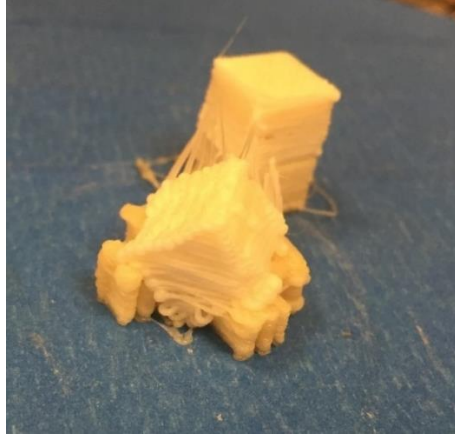


Figure 42. Successfully-printed single-extrusion rotated block with significant oozing.

In response, efforts were taken to improve print quality by controlling and reducing ooze.

5.4. Ooze controls

Oozing can be caused by the unintentional dripping of filament from the hotend due to gravity.

At the end of each print move, excess material would accumulate and cause blobs. This was controlled by adjusting the following settings:

- Retraction/retraction distance: The length of filament that will be retracted from the hotend after a print move. This reduces the pressure in the hotend chamber.
- Extra restart distance: After retraction, the filament will be pushed back to the original starting position (“primed”) before the next print. However, setting this to a negative value will decrease the length of filament pushed back, preventing oozing at the start of the print
- Retraction vertical lift: Moves the nozzle up in the z-direction whenever a retraction is performed
- Retraction speed: Speed at which the retraction and subsequent priming occurs

- Coast at end/coasting distance: Coasting refers to the practice of stopping the propulsion of the filament early, instead allowing momentum and gravity to extrude the filament for the last few millimeters of the print. This allows any oozing to form a part of the print in a productive manner.
- Wipe: while similar to coasting, wiping occurs at the end of a line before retraction— however, wipe still allows for full extrusion during the entire print distance. The hotend doubles back on already-extruded filaments, where any oozing can be captured and distributed.

In order to determine the optimal settings, default values were utilized at first and then refined after trial-and-error. The settings that resulted in minimal oozing are as follows:

Ooze Control			
<input checked="" type="checkbox"/>	Retraction	Retraction Distance	6.00 mm
		Extra Restart Distance	0.00 mm
		Retraction Vertical Lift	0.00 mm
		Retraction Speed	2400.0 mm/min
<input checked="" type="checkbox"/>	Coast at End	Coasting Distance	1.00 mm
<input checked="" type="checkbox"/>	Wipe Nozzle	Wipe Distance	5.00 mm

Figure 43. Ooze control settings.

5.5. Virtual extruder support

Following installation of the new RUMBA printer driver board, the code for G-code based mixing was written into the printer machine commands. This required the custom definition of different virtual extruders in the beginning of each G-code file, assigning a tool number to each desired mixing ratio (Appendix 12.3). This can be done seamlessly by including this code as a default starting script, which will automatically be added to the beginning of each G-code file produced by Simplify3D.

Two primary G-code commands exist in the virtual extruder G-code: M163, which defines the mixing weights (which must add up to 1), and M164, which stores the weight under a given extruder number, followed by the S. As seen below, the fourth large block of code sets 75% weight to Extruder 0, 0.25% weight to Extruder 1, and 0% weight to extruder 2. This specific ratio is then stored as Extruder 3, which is currently unused. Subsequent calls to Extruder 3 will activate this specific stored ratio.

```

G28 ; home all axes

; 100% Lay-felt
M163 S0 P1
M163 S1 P0
M163 S2 P0
M164 S0

; 100% Gel-lay
M163 S0 P0
M163 S1 P1
M163 S2 P0
M164 S1

; 100% PLA
M163 S0 P0
M163 S1 P0
M163 S2 P1
M164 S2

; 75% Lay-felt, 25% Gel-lay
M163 S0 P0.75
M163 S1 P0.25
M163 S2 P0
M164 S3

```

Figure 44. Incorporation of virtual extruder G-code into the default starting script settings. M163 sets the weights of the extruded materials, while M164 defines those weights with a virtual extruder number following the S. Hence, anytime

A complete listing of the extruders is below:

Extruder 0 (Actual)	100% Gel-lay	Extruder 3 (Virtual)	25% Gel-lay, 75% Lay-felt
Extruder 1 (Actual)	100% Lay-felt	Extruder 4 (Virtual)	50% Gel-lay, 50% Lay-felt
Extruder 2 (Actual)	100% PVA (Support)	Extruder 5 (Virtual)	75% Gel-lay, 25% Lay-felt

Table 5. Virtual extruder references.

5.6. Marlin Firmware Configuration

Marlin is a highly-customizable, open-source 3D printer firmware. To begin the firmware configuration process, the board was installed on a computer using the RUMBA Taurino USB driver [27]. The most recent version of the Arduino IDE [28] was also installed, since the RUMBA has an Arduino-based chip. Lastly, the Marlin firmware itself needed to be downloaded.

Throughout the process, multiple versions of Marlin were configured with unsuccessful printing. Eventually, it was discovered that the most recent development version, build 1.1.0-RCBugFix, fixed several bugs in the firmware that prohibited the proper functioning of the virtual extruder support functionality discussed in Section 5.5. After downloading the proper version, the first step in configuring the Marlin firmware involved replacing the standard Configuration.h and Configuration_adv.h files in the Marlin directory with the respective files from the ~\Marlin-RCBugFix\Marlin\example_configurations\delta\generic directory. These files allow for the configuration of a delta-geometry printer.

Afterwards, the following settings were adjusted in Configuration.h:

- Change the MOTHERBOARD value to BOARD_RUMBA.
- Define the number of extruders as 1. This can be confusing—although there are technically 3 extruder motors, the software is specifying the number of hotends in this instance.
- Uncomment the #define MIXING EXTRUDER line to enable the mixing extruder feature. #define MIXING STEPPERS 3, MIXING VIRTUAL TOOLS 16. Although 16 is more virtual extruders than we need, there is no penalty to leaving the option open to potentially integrate more virtual tools in the future.

- TEMP_SENSOR_0 should be 1.
- Delta geometry settings: DELTA_DIAGONAL_ROD 197.0, DELTA_SMOOTH_ROD_OFFSET 157.0, DELTA_EFFECTOR_OFFSET 50.0, DELTA_CARRIAGE_OFFSET 28.0, DELTA_PRINTABLE_RADIUS 70.0. These were measured with a ruler according to the diagram below.

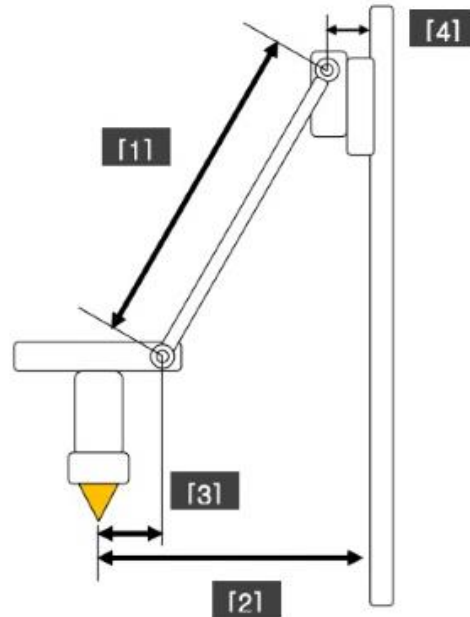


Figure 45. Delta printer geometry. Measurements include DELTA_DIAGONAL ROD [1], DELTA_SMOOTH_ROD_OFFSET [2], DELTA_EFFECTOR_OFFSET [3], and DELTA_CARRIAGE_OFFSET [4]. DELTA_PRINTABLE_RADIUS is based on the manufacturer specification of 70 mm. These measurements are inputted into the Configuration.h file.

- Set all ENDSTOP_INVERTING values to false to prevent the inversion of endstop logic.
- Change DEFAULT_AXIS_STEPS_PER_UNIT to {80, 80, 80, 100}. The values of 80 were calculated based on the below formula, while the value of 100 was determined through experimental trial-and-error with the default values. According to Geeetech, *motor steps per rev* is 200 (which refers to the number of steps for one full revolution of the motor), and the *driver microstep* is 16 (meaning each full step can be broken into 16 smaller steps with software). *Belt pitch*, or the distance between

teeth on the timing belt, is 2mm, and the axis pulley has 20 teeth. These values are based on direct measurements.

$$\text{steps/mm} = \frac{\text{motor steps per rev} * \text{driver microstep}}{\text{belt pitch} * \text{pulley number of teeth}}$$

- Set DEFAULT_MAX_FEEDRATE TO {200, 200, 200, 25} to limit the printer against extremely fast movements. Similarly, change DEFAULT_MAX_ACCELERATION to {7000, 7000, 7000, 10000} to avoid rapid accelerations.
- MANUAL_Z_HOME_POS should be 31 to account for the shortened height of the printer.
- Uncomment REPRAP_DISCOUNT_SMART_CONTROLLER to enable the display.

Once changes were made, the code was compiled in Arduino. The updated firmware was uploaded to the board by clicking “upload” in the Arduino GUI after connecting the RUMBA board to the computer via USB. A message in Arduino will indicate that the upload is complete. The printer will restart itself if plugged in and turned on.

6 Block Printing & Assembly

6.1 Design and Printing of Prototype

Overall, the number of printer hardware and software modifications needed exceeded expectations. The project became more heavily focused on the design and construction of the printer, which delayed the fabrication of the phantom itself. The ability to print rotated, mixed cubes was not achieved until the week of March 20, 2017 due to the hardware and software complexity of controller board replacement.

Despite the delays, a simple prototype phantom was successfully constructed to provide a proof-of-concept. This phantom consists of 22 non-rotated cubes of 11 different filament ratios, ranging from a 100%/0% Lay-felt/Gel-lay ratio to a 0%/100% Lay-felt/Gel-lay ratio in increments of 10%. These blocks were placed into the hydrogel suspension in the same orientation to assess the directionality of the diffusion.

Blocks were printed using the original non-rotated G-code generated by Slic3r and manually modified to obtain parallel infill lines. After printing, the cubes were carefully removed from the build plate with a putty knife and placed in a distilled water bath for two days to allow for the dissolution of carrier filament. Throughout the process, cubes were clearly separated and labeled to prevent misplacement, as many appear identical. Caution must be exercised to prevent distortion or breaking of the blocks.

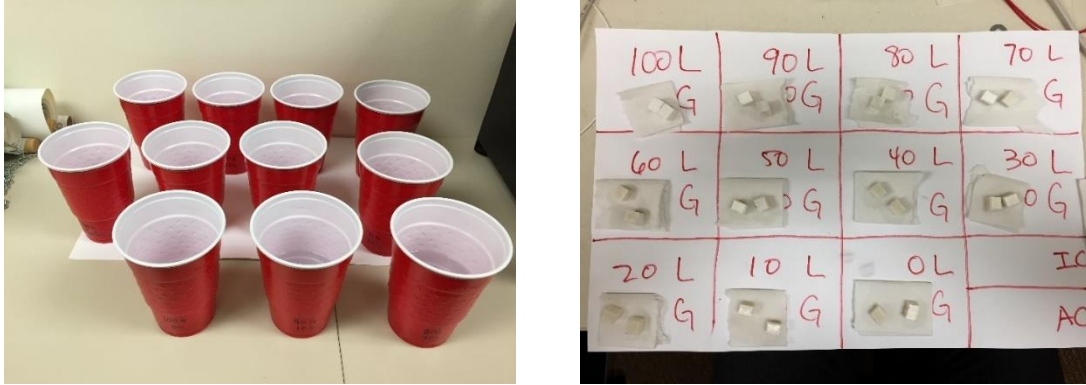


Figure 46. Placement of blocks in water for removal of carrier filament (left). After two days, cubes were removed from the water for placement into the hydrogel suspension (right).

6.2. Design and Fabrication of a Bath Frame

The 1-4 day waiting period for the carrier filament to dissolve in a water bath is a time-consuming process. An email exchange between Kai Parthy, the inventor of Gel-lay and Lay-felt, revealed that the process may be faster when blocks are exposed to agitation and increased water temperature. However, the parallel structures of the blocks make them susceptible to breakage upon excessive agitation. To allow for the flow of water around the part without excessive block movement, a submersible cube frame was designed and 3D-printed. Newly printed blocks can be placed in the circular frame and submerged in a bucket. The frame accommodates space for a magnetic stir bar in the center, and the circular design allows for maximum surface area contact between the cube and circulating water. This design also ensures maximum separation between blocks to maximize flow and surface area contact.

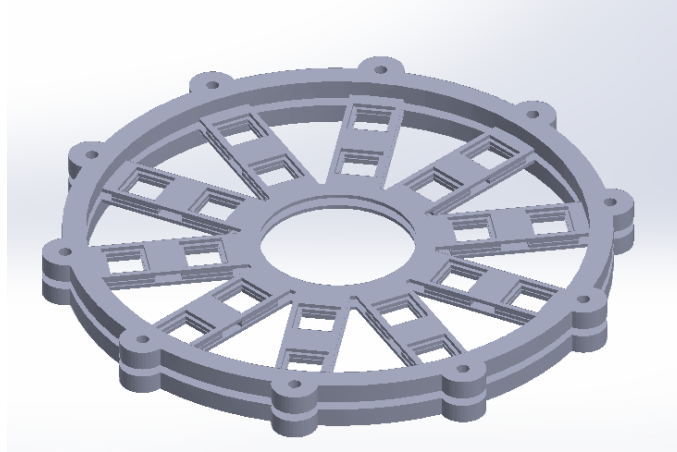


Figure 47. Circular bath frame designed in Solidworks. Blocks are placed between the two wheel halves and secured with screws. Cubes are kept in place with lips that minimally impede exposure to water. Circular center allows for stir bar movement.

6.3. Preparation of Suspension Medium and Block Placement

Following the prototype described in Chapter 3, it was evident that a larger amount of block suspension hydrogel would be required for the MR scanner to register a signal. In this revised design, 2L of hydrogel was made in a 15L plastic bin according to the same formulation and procedure outlined in Chapter 3. The hydrogel was left overnight to stiffen and was placed in a vacuum chamber to remove bubbles. The clear, viscous gel, relatively free of bubbles, was transferred into the phantom vessel, a plastic container 13cm wide, 16cm long, and 13cm deep.

Using forceps, the cubes were then carefully inserted into the prepared hydrogel in the same orientation, with fibers aligned in the anterior-posterior direction. All cubes were inserted approximately 2 cm below the surface of the hydrogel to maintain cube visibility. Cubes of the same ratio were placed closer together, with a separation distance of approximately 1cm to prevent diffusion interference. In the container, sets of cubes were arranged in decreasing order based on Lay-felt proportion from left-to-right and top-to-bottom, in “reading order.”.

Afterwards, the surface of the hydrogel was smoothed and any visible bubbles were removed with a syringe and needle.



Figure 48. Forceps were used to place blocks within the gel (left). The completed phantom prototype (right) consisted of three rows of cubes. The first and second rows each had four pairs of blocks, while the third row had three pairs of blocks, for a total of 22 blocks. Blocks are arranged in decreasing Lay-felt proportion from left to right within each row, with the top row containing the highest Lay-felt proportions and the bottom row containing the lowest Lay-felt proportions.

7 Block Measurement & Analysis

Block scanning was performed using two Siemens Prisma MRI scanners. Original scanning occurred at the MGH Martinos Center for Biomedical Imaging in Bay 4. A second scan of the same phantom occurred approximately three weeks later at the Center for Brain Science Neuroimaging Facility in the Northwest Building at Harvard.

The phantom was supported in the head coil with foam blocks on the bottom and wedges on either side. Diffusion studies were conducted with a 32-channel head coil and 64 diffusion directions, 1.1x1.1x1.1 mm voxels, and anterior-posterior phase encoding. Complete scanning configurations are included in Appendix 12.2. Scans were made in the coronal plane, such that a cross section would capture blocks in the x-y plane at the same point on the Z-axis. Scans lasted approximately 14 minutes at MGH, while scans were approximately 10 minutes at Harvard due to modifications in the protocol.

Results from the MGH scans were interpreted offline using ImageJ, while results from the Harvard scans were interpreted directly using the Siemens MRI software.

7.1. Anisotropy Measurements and Analysis

In the DTI studies, anisotropy is visualized using fractional anisotropy (FA) maps. In this scan, brighter regions correspond to higher levels of anisotropy and higher FA values; conversely darker regions correspond to more isotropic diffusion and lower FA values. The FA map from the MGH DTI study is reproduced below. At first glance, the two blocks in in Box A represent high levels of anisotropy, as evidenced by their relative brightness. In contrast, blocks in Box K

are much less bright, representing more isotropic diffusion. In general, the blocks follow this trend as the proportion of Lay-felt decreases and the proportion of Gel-lay increases.

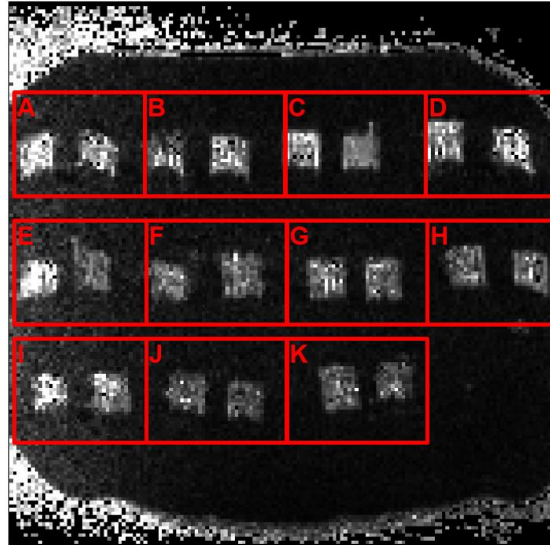


Figure 49. FA-map of phantom prototype performed at MGH. Greater brightness intensity corresponds to higher FA value. General pattern of decreasing intensity from A-K.

A-K: Samples of 11 different ratios, each with $N = 2$. Box A contains 2 blocks of 100% Lay-felt / 0% Gel-lay. Successive boxes decrease in Lay-felt proportion by 10% and correspondingly increase in Gel-lay proportion by 10%. Box K contains 2 blocks of 0% Lay-felt / 100% Gel-lay.

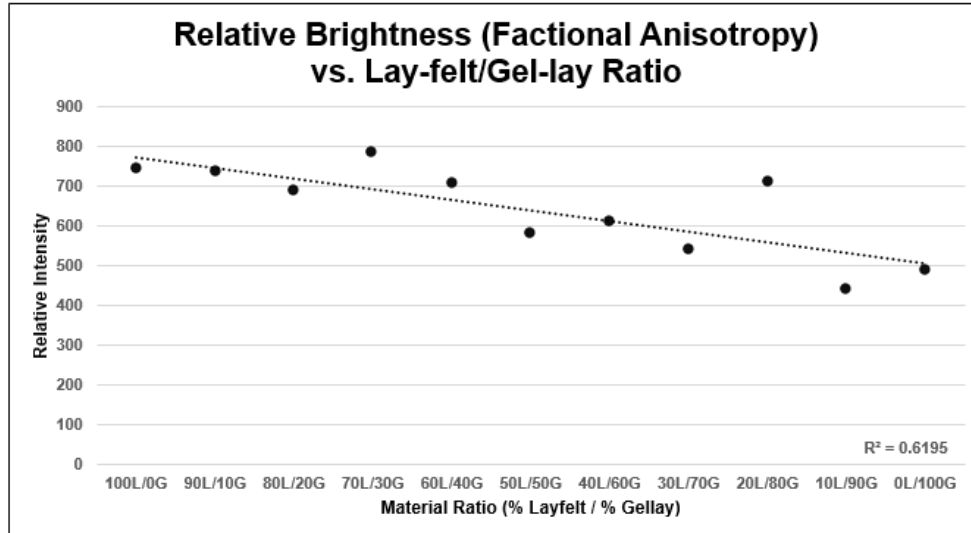
Within this phantom, two blocks were mistakenly not aligned at the same depth as others, as they were placed too deep into the gel. As a result, the original FA scans did not depict all blocks along the same z-axis slice. The above image has thus been post-processed to superimpose the images of the two blocks located more deeply, though this does not impact the accuracy of the above image in depicting FA values. Furthermore, blocks along the leftmost edge of the phantom seem to be uncharacteristically brighter than their counterparts, which suggests systematic error along that edge. This can be explained by the protrusion of the phantom out of the measurement head coil, leading to a poorer-quality signal along that edge. This “edge effect” is confirmed by the presence of noise along the outside perimeter of the phantom vessel.

Quantitative Analysis

Although brightness seems to generally decrease, it is important to quantify the relative brightness of the blocks and demonstrate whether the coefficient relating Lay-felt ratio to brightness is statistically significant. Quantification of brightness was performed using ImageJ.

First, the entire image sequence of IMA files was imported into ImageJ. Afterwards, twenty-two different regions of interest (ROIs) measuring 10mm×10mm were manually identified on the FA map based on block locations. Brightness analysis for each region of interest was performed using the Multi Measure tool, which analyzed the brightness data of each ROI independently. For each set of blocks, the maximum brightness values were extracted, averaged, and plotted against its corresponding Lay-felt proportion. Maximum brightness values are used because these values typically correspond to the center of the block, which is the area of interest when analyzing an FA slice image. An analysis of brightness profiles, which plots brightness against slice number, reveals that maximum brightness values are quite representative of the entire block as a whole (Appendix 12.4).

Because of the edge effect along the leftmost region of the phantom, regressions were performed with and without the data pertaining to the three leftmost blocks. However, in both cases, the coefficients were statistically significant at the 5% level. This suggests that the error does not have a large bearing on the interpretive value of this study. For the purposes of this report, blocks confounded by edge effects were discounted from the data.



Notes:

Heteroskedasticity-robust regression coefficient on Lay-felt proportion: 2.93 (p < .01).

95% CI: (14.01, 44.50) *Rel. Intensity = 516.54 + 2.93 × (Lay-felt %)*

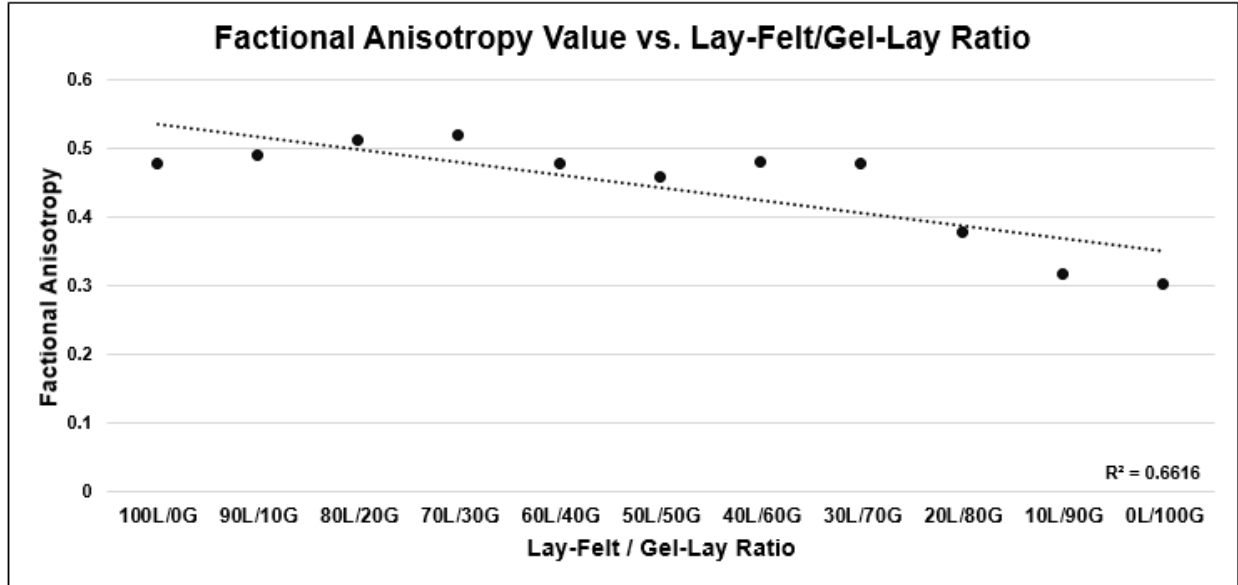
Brightness values: Averaged maximum brightness values for N = 2 blocks of each treatment.

Figure 50. Anisotropy, represented by brightness, is directly correlated with Lay-felt proportion and inversely correlated with Gel-lay proportion. This relationship is statistically significant at the 1% level.

The above chart strongly suggests a causal relationship between Lay-felt proportion and degree of anisotropy. The coefficient on Lay-felt proportion is 2.93, which can be interpreted in the following way: on average, for a one percentage point increase in the Lay-felt proportion, the relative intensity increases by 2.93. The constant term in the regression suggests that the minimum achievable brightness is approximately 516.54. This graph demonstrates proof-of-concept for the phantom design, as it confirms the theory that Lay-felt results in more anisotropic diffusion than Gel-lay.

However, because ImageJ is not radiological software, it is difficult to obtain direct FA measurements. To address this issue, a second set of scans of the phantom was performed at Harvard, with voxel sizes of 1.1mm and 1.5mm. FA values resulting from the 1.1mm-voxel scan were quantified on-the-spot with the Siemens MRI software. This was done by overlaying a

region of interest on the FA scan and obtaining the average FA value using the built-in measurement tool. The FA values for N = 2 cubes of each ratio were averaged and plotted below.



Notes:

Heteroskedasticity-robust regression coefficient on Lay-felt %: 0.19 (p < .01).

FA = 0.350 + 0.00187 × (Lay-felt %)

Figure 51. FA data from Harvard scan. Similar to the MGH scan, the correlation coefficient between FA value and Lay-felt proportion is statistically significant at the 1% level.

From this chart and corresponding regression, it is evident that the relationship between fractional anisotropy and Lay-felt ratio is statistically significant, as before. In addition, a comparison between the Harvard scan and the MGH scan reveal that the data shape are consistent, which offers two implications: 1) that the phantom is generally able to retain its diffusive properties over time, and 2) that the methodologies for measuring anisotropies are mutually validating.

Furthermore, this second study sheds light on the range of FA values that are able to be capitulated by the current phantom. Physiological FA values of the human brain are typically in the 0.4 – 0.7 range [11], which partially overlaps with the phantom’s current range of 0.3 – 0.5.

Future modifications to the phantom design—such as infill density during 3D printing, layer

thickness, layer width, and water bath soaking time—may be able to bring the phantom’s FA range closer to physiological values.

7.2. Diffusion Direction

Diffusion direction is visualized with Color Fractional Anisotropy (Color FA). In a Color FA map, green corresponds to anterior-posterior diffusion (i.e. diffusion along the z-axis).

Quantitatively, the coloring within an FA map can be described by trigonometric equations. The direction of the major diffusion eigenvector (v_1) determines the hue (color), while the FA value determines the brightness.

Specifically, if we measure the angle formed between the major diffusion eigenvector (v_1) and the Cartesian x-, y-, and z-axes and assign them values of α , β , and γ , respectively, we can characterize the color scheme of an FA map with the following equations:

$$\begin{aligned} Red &= FA \times \cos(\alpha) \\ Blue &= FA \times \cos(\beta) \\ Green &= FA \times \cos(\gamma) \end{aligned}$$

In the case of this phantom, cubes were positioned such that tracts were mostly parallel with the Cartesian z-axis, corresponding to anterior-posterior diffusion within the body. The results reveal that the cubes generally appear to be green, consistent with the way in which they were placed in the gel. This makes mathematical sense, as γ —the angle between the major diffusion direction and the Cartesian z-axis—should be small. The cosine of a small angle should be close to 1, thereby preserving the FA value. In contrast, the major diffusion direction should be orthogonal to both the x- and y-axes, which induces α and β to approach 90° . The cosine of a right angle approaches zero, thereby eliminating the red and blue hues.

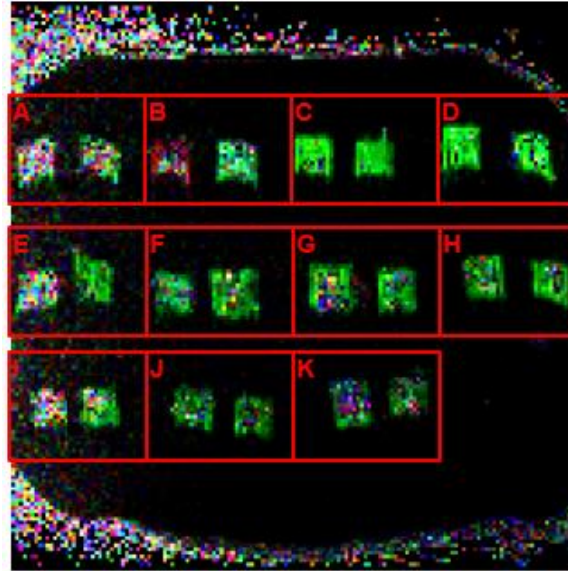


Figure 52. Color FA map of the prototype phantom. Green: Anterior/posterior diffusion, Blue: Superior/inferior diffusion, Red: Left/right diffusion. Cubes show significant A/P diffusion.

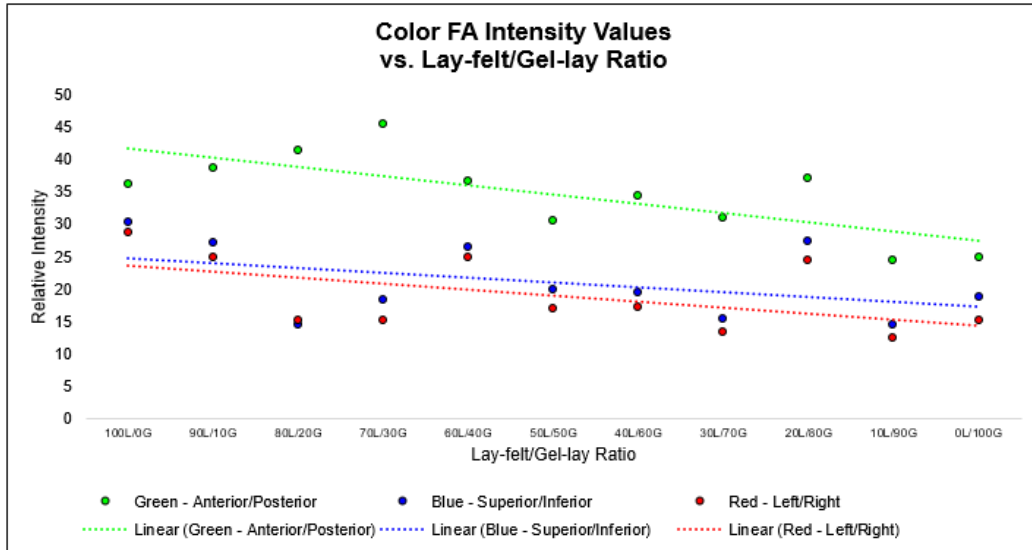
A-K: Samples of 11 different ratios, each with $N = 2$. Box A contains 2 blocks of 100% Lay-felt / 0% Gel-lay. Successive boxes decrease in Lay-felt proportion by 10% and corresponding increase in Gel-lay proportion by 10%. Box K contains 2 blocks of 0% Lay-felt / 100% Gel-lay.

From qualitatively observing the above, it is evident that most blocks appear to be green. However, the left block in Box B appears to be red, which suggests with diffusion in the x-direction. Re-inspection of the phantom after scanning revealed that the corresponding block was improperly placed, with fibers parallel to the Cartesian x-axis. While this circumstance was unintentional, it did provide an additional means to verify consistency. Qualitatively, the coloring demonstrated by this study is consistent with the way in which cubes were placed into the hydrogel, demonstrating that diffusion direction is effectively controlled by printing direction.

Quantitative Analysis

Quantitative analysis of these data were performed using ImageJ. After importing the color FA images into the software, the Image > Color > Split Channels tool was used to isolate the red,

green, and blue components. Following isolation of each color channel, a brightness analysis was performed on each in a process similar to Section 7.1.



Heteroskedasticity-robust regression coefficients:

Green: 0.144 (p = .011) Red: 0.092 (p = 0.079) Blue: 0.075 (p = 0.186)

Figure 53. Quantitative analysis of Color FA data, with the intensity of each color channel plotted against block ratios. The intensity of the green (anterior/posterior) data dominates, while the red and blue data are both at similar substantially lower levels. Only the regression coefficient on the green data is significant at the 5% level.

The data quantitatively demonstrate that diffusion in the anterior/posterior direction (green) dominates over diffusion in the left/right (red) and superior/inferior (blue) directions. Additionally, not only are the red and blue intensities lower than the green, but they are also equally lower. This is consistent with our expectations, since diffusion in one Cartesian direction is orthogonal to both other directions. Lastly, only the regression coefficient on the green data is statistically significant at the 5% level—meaning there is only a statistically significant relationship between anisotropy and material ratio in the designated direction. We cannot reject the hypothesis that the correlation between intensity and material ratio is zero for the red and blue data, as expected.

Together, these observations provide a strong proof-of-concept for the phantom design. It also provides strong evidence to suggest that the 3D printer is able to consistently manufacture blocks in line with the phantom design inputs. These results are extremely promising for the viability of the printer and of the greater phantom technology as a whole.

8 Budget

Every effort was made to minimize costs throughout the project. Designs that maximized use of existing materials, equipment, hardware, or software were prioritized. In some cases, such as the use of Carbomer/PAA for the hydrogel suspension, this strategy was successful. In other cases, such as slicing software selection, every effort was made to ensure a costly upgrade was necessary.

The relatively inexpensive nature of the printer, however, was also the main source of roadblocks for this project. Because the printer was of lower quality, significant design overhauls were required, preventing the project from developing more deeply into the phantom manufacturing phase as originally intended.

The ~\$600 spent on this project, generously covered by SEAS and the SimGroup at MGH, was able to yield a printer that could provide a very solid proof-of-concept for this phantom design. To mass-produce phantoms of this type, larger investments should be made to develop a heavy-duty system capable of precise, rapid, and automated fabrication. Given the expanding size of the DTI market, large-scale investments may be warranted.

Item	Amount	Funding Source
Geeetech Delta Rostock 301 Printer	\$439.99	SEAS ES100 Budget
Diamond Hotend	\$55.00	SEAS ES100 Budget
Extruder Metal Frame	\$11.94	SEAS ES100 Budget
PVA filament	\$24.99	SEAS ES100 Budget
Steel shafts	\$24.18	MGH lab budget
Miscellaneous electronics, hardware components, materials	\$20.00 (estimated)	MGH lab inventory

9 Conclusion and Future Work

As dual aims, this project sought to (1) construct a novel 3D printer capable of printing small cubes of mixed materials and arbitrary spatial orientations, and (2) use these cubes and other materials to construct a DTI phantom. At the conclusion of this project, the printer was fully constructed, capable of printing all block types necessary for full phantom assembly. A simplified phantom prototype was also constructed, and with the printer now fully functional, the original phantom design goal may only be weeks away.

DTI scans of the phantom prototype provide proof-of-concept for this phantom fabrication technique. The critical properties of anisotropy and direction were effectively controlled by varying material ratios and fiber orientation, and these results were statistically significant. In addition, this project also characterized the properties of Lay-felt and Gel-lay, two novel materials, providing insight into their biomimetic properties.

Over the course of the project, numerous unforeseen mechanical and software issues added complexity and time demands to the project. The identification and diagnosis of dozens of quality issues required the replacement of critical parts, which subsequently resulted in smaller electronic and software compatibility issues. Major modifications—such as firmware configuration and the machining of steel shafts—required the acquisition of new skills. As a first attempt to print with these unprecedented materials and methods, many solutions and best practices required original investigation.

As a first step, further work involves fabricating rotated, mixed cubes with the newly configured controller board and firmware. With this capability, the 3 cube \times 3 cube \times 3 cube phantom can be fully constructed without much additional work.

Following this, many efforts can be focused on the software development front. Custom slicing software would provide a simplified process for G-code generation. Ideally, the software would accept anisotropy and direction parameters as inputs and automatically generate G-code outputs without need for manual post-processing. Further work may also focus on a more robust way of assembling cubes into a physical phantom, as the current model with an open container of hydrogel is prone to movement and damage.

Although the printer is generally capable of printing all types of blocks, many design elements can still be improved. Cleanly-fitting Bowden tube connectors, more secure controller board wiring, and higher-quality build plate fan mounts would enhance the reliability of the printer. Modifications such as automatic plate leveling would allow for easier maintenance and reliability.

Though much work still lies ahead, this project brought together the fields of materials science, mechanical engineering, electrical engineering, and computer science to create a functional low-cost 3D printer. The phantom created by this printer shows high potential for continued success given further work.

10 Acknowledgements

This thesis—and the incredible amounts of learning and growth that accompanied it—would not have been possible without the generosity of many special people.

I would like to thank my advisor, Mark Ottensmeyer, for his continuous teaching, support, and mentorship throughout the project. I am similarly indebted to Bis Mukherjee, Gianluca De Novi, and Damien Galanaud, who were always so astutely able to help with any issue that arose. Their patience, expertise in 3D printing, and willingness to teach directly impacted my ability to complete this project. Moreover, I am highly appreciative of Damien's loan of Simplify3D software and the RUMBA board—two mission-critical components of this project. Filippo Bazuro, an intern in the Group, quickly became my go-to hydrogel expert, and I'm highly appreciative of his help and friendly lab presence.

I would also like to acknowledge Phoebe Chan for her extraordinary generosity in sparing hours of her time to help me configure the MR scanner and acquire images. Being able to get scanner time at the Martinos Center is nothing short of a small miracle, and Phoebe has been willing to share that time with me. Ross Mair at Harvard has also been an extremely valuable resource, giving me the opportunity to use Harvard's MRI equipment while learning from an industry expert.

The ES 100 staff has also been a constant source of wisdom and support. Anas Chalah and Karena McKinney, my section leaders, provided incredible feedback. And although hearing constructive feedback can be frustrating, this project would not have been a success without their input. Lastly, I am grateful to Rob Wood, my thesis reader, for his keen interest and involvement in my project, as well as his leadership of the ES 100 course.

11 References

- [1] A. L. Alexander, J. E. Lee, M. Lazar and A. S. Field, "Diffusion Tensor Imaging of the Brain," *Neurotherapeutics*, vol. 4, no. 3, p. 316–329, 2008.
- [2] I. D. Croall, C. J. Cowie, J. He, A. Peel, J. Wood, B. Aribisala, P. Mitchell, A. D. Mendelow, F. E. Smith, D. Millar, T. Kelly and A. M. Blamire, "White matter correlates of cognitive dysfunction after mild traumatic brain injury," *Neurology*, vol. 83, no. 6, pp. 494-501, 2014.
- [3] T. Zhu, R. Hu, X. Qiu, M. Taylor, Y. Tso, C. Yiannoutsos, B. Navia, S. Mori, S. Ekholm, G. Schifitto and J. Zhong, "Quantification of Accuracy and Precision of Multi-Center DTI Measurements: A Diffusion Phantom and Human Brain Study," *Neuroimage*, vol. 56, no. 3, p. 1398–1411, 2011.
- [4] S. Gouttard, M. Styner, M. Prastawa, J. Piven and G. Gerig, "Assessment of Reliability of Multi-site Neuroimaging via Traveling Phantom Study," *Med Image Comput Comput Assist Interv.*, vol. 11(Pt 2), p. 263–270, 2008.
- [5] C. Jiang, L. Zhang, C. Zou, X. Long, X. Liu, H. Zheng, W. Liao and Y. Diao, "Diurnal Microstructural Variations in Healthy Adult Brain Revealed by Diffusion Tensor Imaging," *PLOS ONE*, vol. 9, no. 1, p. e84822, 2014.
- [6] American College of Radiology, "acr.org," 2015. [Online]. Available: https://www.acr.org/~media/ACR%20No%20Index/Documents/QC%20Manual/2015_MR_QCManual_Book.pdf. [Accessed February 2017].
- [7] E. Palacios, A. Martin, M. Boss, F. Ezekiel, Y. Chang, E. Yuh, M. Vassar, D. Schnyer, C. MacDonald, K. Crawford, A. Irimia and P. M. A.W. Toga, "Toward Precision and Reproducibility of Diffusion Tensor Imaging: A Multicenter Diffusion Phantom and Traveling Volunteer Study," *American Journal of Neuroradiology*, vol. 10.3174/ajnr.A5025, 2016.
- [8] L. O'Donnell and C.-F. Westin, "An introduction to diffusion tensor image analysis," *Neurosurg Clin N Am*, vol. 22, no. 2, p. 185–viii, 2012.
- [9] Organisation for Economic Co-operation and Development, "OECD Data," 2014. [Online]. Available: <https://data.oecd.org/healthqt/magnetic-resonance-imaging-mri-units.htm>. [Accessed February 2017].
- [10] J. M. Soares, P. Marques, V. Alves and N. Sousa, "A hitchhiker's guide to diffusion tensor imaging," *Frontiers in Neuroscience*, vol. 7, no. 31, 2013.
- [11] M. Rosenbloom, E. V. Sullivan and A. Pfefferbaum, "Using Magnetic Resonance Imaging and Diffusion Tensor Imaging to Assess Brain Damage in Alcoholics," National Institutes of Health, 2004.
- [12] P. J. Bassera and C. Pierpaoli, "Microstructural and physiological features of tissues elucidated by quantitative-diffusion-tensor MRI," *Journal of Magnetic Resonance*, vol. Series B, no. 111, pp. 209-219, 1995.
- [13] "MatterHackers," [Online]. Available: <http://www.matterhackers.com/store/3d-printer-filament/poro-lay-lay-felt-porous-filament-1.75mm>. [Accessed 1 October 2016].

- [14] "MatterHackers," [Online]. Available: <https://www.matterhackers.com/store/3d-printer-filament/poro-lay-gel-lay-porous-filament-175mm>. [Accessed 1 October 2016].
- [15] A. Hellerbach, V. Schuster, A. Jansen and J. Sommer, "MRI Phantoms – Are There Alternatives to Agar?," *PLOS One*, vol. 8, no. 8, p. e70343, 2013.
- [16] N. Saha, C. Monge, V. Dulong, C. Picart and K. Glinel, "Influence of Polyelectrolyte Film Stiffness on Bacterial Growth," *Biomacromolecules*, vol. 14, no. 2, pp. 520-528, 2013.
- [17] B. Warfield, "CAD Survey Results: Market Share," CNC Cookbook, 27 January 2016. [Online]. Available: <http://blog.cnccookbook.com/2016/01/27/cnccookbook-2016-cad-survey-results-part-1-market-share/>.
- [18] RepRap.me, "RUMBA," [Online]. Available: <http://www.reprap.org/wiki/RUMBA>. [Accessed 28 3 2017].
- [19] M. Firmware, "GitHub," 6 December 2016. [Online]. Available: <https://github.com/MarlinFirmware/Marlin/tree/RCBugFix>.
- [20] Geeetech, "Geeetech.com," 20 July 2016. [Online]. Available: http://www.geeetech.com/wiki/images/4/44/Geeetech_Rostock_301_User_Manual.pdf. [Accessed 1 November 2016].
- [21] Banggood, "3D Printer MK8 1.75mm Remote Extruder Metal Frame Kit For Makerbot Reprap," [Online]. Available: http://www.banggood.com/3D-Printer-MK8-1_75mm-Remote-Extruder-Metal-Frame-Kit-For-Makerbot-Reprap-p-1070154.html?rmmds=search. [Accessed 15 11 2016].
- [22] Micro Center, "Inland 1.75mm 3D Printer Cleaning Filament," [Online]. Available: http://www.microcenter.com/product/442003/175mm_3d_printer_cleaning_filament. [Accessed 25 11 2016].
- [23] Geeetech, "Geeetech Forums," [Online]. Available: <http://www.geeetech.com/forum/viewtopic.php?f=19&t=18149&p=32649>. [Accessed 26 11 2016].
- [24] McMaster-Carr, [Online]. Available: <https://www.mcmaster.com/#5544t312/=15w9k17>. [Accessed 15 01 2017].
- [25] Raoulito9, "Thingiverse," 19 June 2016. [Online]. Available: <http://www.thingiverse.com/thing:1634366>. [Accessed 20 1 2017].
- [26] Raoulito9, "Rostock 301 Layer Fan Support," Thingiverse, 28 November 2016. [Online]. Available: <http://www.thingiverse.com/thing:1922986>. [Accessed 20 January 2017].
- [27] RepRap.me, "RUMBA TAURINO Driver Setup," [Online]. Available: http://www.reprap.org/wiki/File:RRD_RUMBA_TAUINO_DriverSetup.zip. [Accessed 15 03 2017].
- [28] Arduino, "Arduino Software," [Online]. Available: <https://www.arduino.cc/en/Main/Software>. [Accessed 15 3 2017].
- [29] J. E. L. M. L. A. S. F. Andrew L. Alexander, "Diffusion Tensor Imaging of the Brain," *Neurotherapeutics*, vol. 4, no. 3, p. 316–329, 2007.
- [30] RepRap.me, "Diamond Hotend," 10 April 2015. [Online]. Available: http://reprap.org/wiki/File:Diamond_Hotend_Step_7.JPG. [Accessed 28 3 2017].

- [31] Core Commerce, [Online]. Available:
<https://www19.corecommerce.com/~twintecinc493/uploads/small%20frame.jpg>. [Accessed 28 3 2017].
- [32] Singcore, [Online]. Available: <http://singcore.com/wp-content/uploads/2015/09/T-Slot-Panels-standard-4-slot-T-Slot-aluminum-extrusion.jpg>. [Accessed 28 3 2017].
- [33] Aus3D.com, "Radial blower fan," [Online]. Available:
<http://aus3d.com.au/image/cache/catalog/products/fans/blower-1600px-600x315.jpg>. [Accessed 29 3 2017].
- [34] RepRap.me, "RUMBA," [Online]. Available:
<http://www.reprap.org/mediawiki/images/thumb/1/17/Rumba4.jpg/500px-Rumba4.jpg>. [Accessed 29 3 2017].
- [35] Aliexpress, "Diamond Hotend Schematic," [Online]. Available:
<https://ae01.alicdn.com/kf/HTB13I1OLpXXXXa7XVXXq6xXFXXXm/Reprap-3D-Printer-Diamond-Hotend-Multi-Color-Hot-End-3-IN-1-OUT-Extruder-HotEnd-full.jpg>. [Accessed 28 3 2017].

12 Appendix

12.1. Slic3r Settings for Non-rotated Cubes

Parameter	Value	Parameter	Value
Layer Height	0.4 mm for all layers	Support material	None
Vertical Shells	0 perimeters	Speed for non-print moves	100 mm/s
Horizontal Shells	0 top/bottom	Infill extruder	1
Infill	80%, line, rectilinear	Support material extruder	3
Skirt and Brim	2 loops, 15 mm from object, 1 layer high	Extrusion width	Default, 150% first layer
Infill speed	50 mm/s		

12.2. Links to Code

[G-code for Rotated Cube](#)

[G-code for Non-rotated Cube](#)

[DTI Scanner Configurations](#)

12.3. Virtual Extruder G-Code

```
;100% Lay-felt
```

```
M163 S0 P1
```

```
M163 S1 P0
```

```
M163 S2 P0
```

```
M164 S0
```

```
;100% Gel-lay
```

```
M163 S0 P0
```

```
M163 S1 P1
```

```
M163 S2 P0
```

```
M164 S1
```

```
;100% PLA
```

```
M163 S0 P0
```

```
M163 S1 P0
```

```
M163 S2 P1
```

```
M164 S2
```

```
;75% Lay-felt, 25% Gel-lay
```

```
M163 S0 P0.75
```

```
M163 S1 P0.25
```

```
M163 S2 P0
```

```
M164 S3
```

```
;50% Lay-felt, 50% Gel-lay
```

```
M163 S0 P0.5
```

```
M163 S1 P0.5
```

```
M163 S2 P0
```

```
M164 S4
```

```
;25% Lay-felt, 75% Gel-lay
```

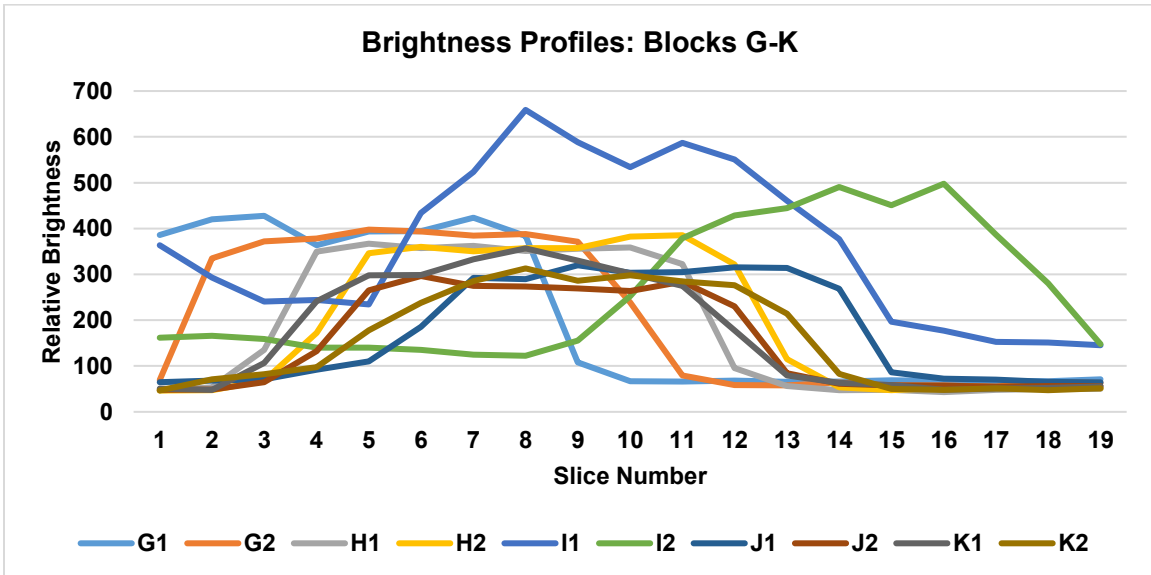
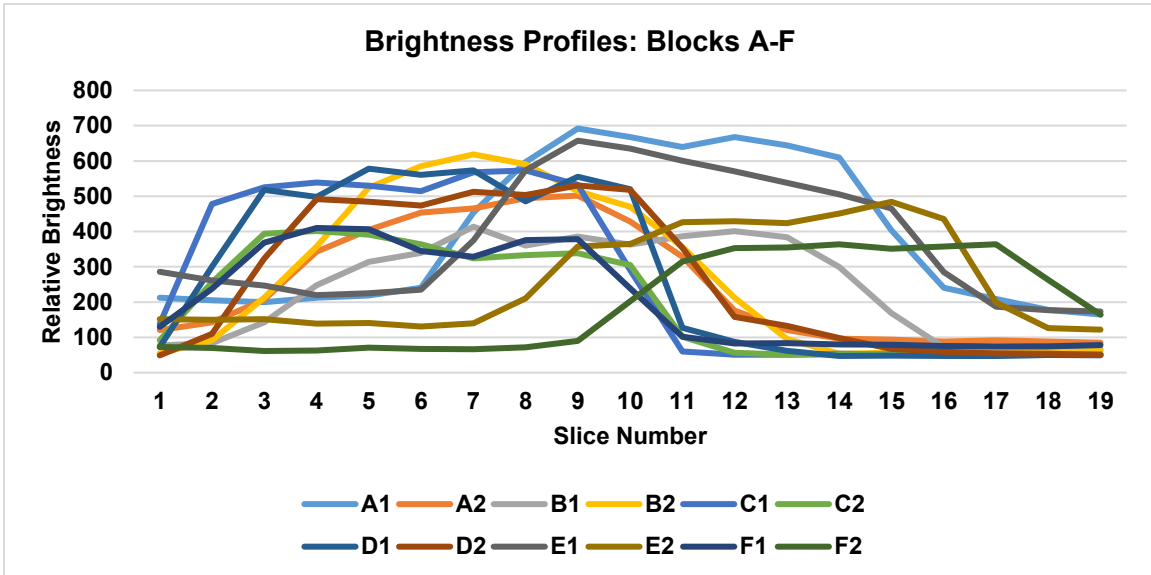
```
M163 S0 P0.25
```

```
M163 S1 P0.75
```

```
M163 S2 P0
```

```
M164 S5
```

12.4. Brightness Profiles



Brightness profiles indicate the representative nature of the maximum brightness value in representing the overall brightness of the block, as plateau behavior is exhibited.